博士論文

Lipodystrophy and cold intolerance in mice lacking *Cnot3* in adipose tissue-specific manner

(脂肪組織特異的 *Cnot3* 欠損マウスに見られる脂肪異栄養症と寒冷不耐症)

李　雪

Contents

Abstract	3-4
Introduction	5-8
Materials and Methods	9-18
Results	19-31
Discussion	32-37
References	38-50
Acknowledgements	51-53
Figures	54-87

Abstract

Lipodystrophy is a pathological state characterized by a complete or partial loss of adipose tissue that, occurs in combination with lipid accumulation in ectopic sites in the body. Patients with lipodystrophy suffer from metabolic consequences, including severe insulin resistance, dyslipidemia, hepatic steatosis, and diabetes mellitus. Elucidation of the mechanisms underlying lipodystrophy is expected to help develop therapeutic strategies for lipodystrophy and related metabolic complications.

CNOT3 is a non-catalytic component of the mammalian CCR4-NOT deadenylase complex, whose molecular and physiological functions remain to be established. Accumulating data suggest that one role of CNOT3 may be related to the control of energy metabolism. In this study, I depleted the *Cnot3* gene specifically in mouse adipose tissues to address its physiological significance in energy metabolism. The loss of CNOT3 caused a marked reduction in the amount of white adipose tissue, by contrast, loss of CNOT3 caused hypertrophy of brown adipose tissue containing fat-laden cells resembling immature white adipocytes. Furthermore, depletion of CNOT3 from adipose tissues induced hyperinsulinemia and hyperglycemia that were associated with insulin resistance and glucose intolerance. Accordingly, plasma triglyceride levels were

elevated and lipids accumulated ectopically in the liver. These results suggested that CNOT3 depletion in adipose tissues generated many of the features of lipodystrophy. I further found that CNOT3 depletion increased apoptosis in peripheral adipocytes and was associated with aberrant fat storage and lipid release; these changes could be a direct cause of the lipodystrophic phenotype of adipose tissue-specific *Cnot3* knockout mice. Finally, to better define the observed lipodystrophic phenotypes, I compared the gene expression profiles of adipose tissue-specific *Cnot3* knockout mice and two phenotypically similar lipodystrophic mouse models, *aP2-nSrebp1c* mice, which overexpress SREBP1, and $Pparg^{ldi/+}$ mice, which conditionally overexpress PPARγ. The results revealed a substantial overlap in gene aberrations that could define a common signature of lipodystrophy.

By revealing the lipodystrophic phenotype caused by the deletion of Cnot3 specifically in adipose tissue, this study provides a novel fundamental basis for better understanding the physiological significance of CNOT3 in the control of energy metabolism Furthermore, the results of this study raise the intriguing possibility that CNOT3 and the CCR4-NOT deadenylase complex could serve as therapeutic targets to treat lipodystrophy.

Introduction

Adipose tissue has two essential biological roles in controlling energy balance and lipid homeostasis: first, it is the major storage site of excess energy in the form of triglycerides and, second, it is an important endocrine organ that synthesizes and secretes hormones and adipokines (Kershaw and Flier, 2004). Dysfunction of adipose tissue can result in not only obesity (an excess of adipose tissue) but also lipodystrophy (a deficiency of adipose tissue). Although these two conditions are opposite pathological states of adipose tissue mass, they are both accompanied by similar metabolic consequences, including dyslipidemia, hepatic steatosis, severe insulin resistance, and diabetes mellitus (Figure 1). Lipodystrophy can be caused by either genetic or acquired factors and can be classified as either generalized or partial, depending on the degree and locality of the fat (Garg A., 2000). Currently, the most common form of lipodystrophy is induced by the protease inhibitors used to treat HIV-infected AIDS patients (Hegele et al., 2007; Caron-Debarle et al., 2010) and affects up to 50% of the patients. Thus, elucidating the mechanisms that underlie lipodystrophy is extremely important for developing therapeutic strategies for not only lipodystrophy but also related metabolic complications.

The CCR4-NOT complex is an evolutionarily conserved complex that has been implicated in the control of multiple steps of mRNA metabolism, including repression and activation of transcription, elongation of mRNA, and deadenylation and subsequent degradation of mRNA (Collart, 2012). Given these diverse activities, it is not surprising that this complex is relevant to a wide range of biological functions. The CCR4-NOT complex plays important roles in cell proliferation, apoptosis, oogenesis and embryogenesis, spermatogenesis, heart function, bone formation and energy metabolism (Collart, 2003; Berthet et al, 2004; Nakamura et al., 2004; Nakashima et al. 2007, Morita et al, 2007; Washio-Oikawa et al, 2007). Recent evidence shows that aberrant regulation of this complex causes metabolic abnormality, heart disease, and osteoporosis (Morita et al., 2011; Neely et al., 2010; Watanabe et al., 2014). CNOT3 is a non-catalytic component of the CCR4-NOT complex and is involved in recruitment of the CCR4-NOT to the 3' end of specific mRNAs (Morita et al., 2011) (Fig.2). Mice haplodeficient in *Cnot3* are lean because of poor fat accumulation. Liver size white and brown adipose tissues (WAT and BAT, respectively) are reduced in these mice, and adipocytes are smaller than those in wild-type mice (Morita et al., 2011). These data suggest that *Cnot3* has a specific function in liver and adipose tissues. Indeed, a

reduction in CNOT3 levels affects the expression of mRNAs that encode proteins that are important for lipid metabolism, glucose metabolism, oxidative phosphorylation, and growth regulation in the liver (Morita et al., 2011). However, the mechanism by which *Cnot3* regulates the lipid metabolism in adipose tissue remains unknown.

In this study, to understand the role of *Cnot3* in adipose tissue, and particularly the relevance of CNOT3 in fat mass and energy metabolism, I specifically depleted *Cnot3* from mouse adipose tissue using the cre/loxP system. I show that mice with adipose tissue-specific depletion of *Cnot3* share many of the features reported in human patients with Congenital Generalized Lipodystrophy (CGL) (Agarwal et al., 2006) and in other lipodystrophy mouse models (Savage, 2009), such as *aP2- nSrebp1c* mice (*Sr*), which express a truncated, constitutively active *Srebp-1c* transgene in adipocytes (Shimomura et al. 1998). These features include a marked reduction in the amount of white adipose tissue, hypertrophy of brown adipose tissue containing fat-laden cells resembling immature white adipocytes, and hyperinsulinemia and hyperglycemia that are associated with insulin resistance and glucose intolerance. Accordingly, plasma triglyceride levels are elevated, and lipid accumulates ectopically in the liver and other

insulin sensitive organs.

I further provide evidence that CNOT3 depletion increased apoptosis in peripheral adipocytes and was associated with aberrant fat storage and lipid release, which could be a direct cause of the lipodystrophic phenotype of mice lacking *Cnot3* in a manner specific to adipose tissue. To examine the underlying mechanisms, I have compared the gene expression profiles of wild-type and mice that lack *Cnot3*in adipose tissue. The results show that pathways involved in apoptosis and inflammation were significantly up-regulated in mice in which *Cnot3* is depleted in adipose tissue. The microarray data also revealed that the expression of SREBP (SREBF) target genes was up-regulated in the adipose tissues of mice in which *Cnot3* is depleted. Taken together, these data suggest that *Cnot3* depletion in adipose tissue confers the lipodystrophic phenotype on mice through apoptosis induction and inflammation and that CNOT3-deficiency contributes to lipodystrophy by regulating a subset of mRNAs, including *Srebp1* mRNA. Thus, CCR4-NOT deadenylase may be a potential therapeutic target for lipodystrophy and the metabolic disorders in HIV-associated lipodystrophy patients.

Materials and Methods

Mice

Generation of *Cnot3*-deficient mice and mice with a floxed *Cnot3* locus (*Cnot3*$^{lox/+}$) were described in previous study (Morita et al., 2011). The *Cnot3*$^{lox/+}$ mice were backcrossed to C57BL/6J mice for at least 8 generations before interbred to generate *Cnot3*$^{lox/lox}$ mice. *Cnot3*$^{ad-/-}$ mice were generated by crossing *Cnot3*$^{lox/lox}$ mice with transgenic mice expressing Cre recombinase under the control of the adiponectin promoter (Eguchi et al., 2011). *Cnot3*$^{lox/lox}$ mice were bred with Adipoq-cre mice to obtain initially heterozygotes *Cnot3*$^{lox/+,cre/+}$. *Cnot3*$^{lox/+,cre/+}$ mice were mated with *Cnot3*$^{lox/lox}$ mice to generate *Cnot3*$^{ad-/-}$ mice. Genotyping was performed by PCR with specific primers as follows: wild-type-5': 5'-CCAGTCTATCTGATGTGGAATTCCTC CATG-3', wild-type-3': 5'-AGGCTGGCAGCTCCTGGAAAGGCTAAGAGG-3', Cre -5': 5'-AGCGATGGATTTCCGTCTCT-3', Cre-5': 5'-CACCAGCTTGCATGATCT CC-3'. PCR amplification of genomic DNA was performed by cycling 30 s at 94 °C, 30 s at 55 °C, 1 min at 72 °C for 40 cycles.

Mice were housed in cages and maintained on a 12-h light–dark cycle, and they had access to water *ad libitum*. Mice were fed a normal chow diet (NCD) (CA-1, CLEA Japan Inc.) or a HFD (HFD32, CLEA Japan Inc.). For fasting analysis, mice were housed individually and deprived of food for 24 h.

For cold exposure experiments, mice were housed individually without food and bedding immediately before the start of experiments. Mice were allowed free access to water and placed at 4 °C while core body temperature was monitored every hour using a rectal probe.

Unless indicated otherwise, male mice at 8–12 weeks of age were used for experiments. Experiments were conducted according to the guidelines for animal use issued by the Committee of Animal Experiments, Institute of Medical Science, University of Tokyo, and Okinawa Institute of Science and Technology Graduated School.

Blood analysis

For glucose tolerance tests, mice were fasted for 16 h. NCD and HFD mice were given an intraperitoneal injection of glucose (0.5 mg/g body weight). For insulin

tolerance tests, NCD mice and HFD mice were given human insulin (1 mU/g body weight). Blood glucose was measured from tail blood using the glucose oxidase method (Sanwa Kagaku). Levels of serum triglycerides and insulin were determined using a Triglyceride E-Test (Wako) and a Mouse Insulin ELISA Kit (Morinaga), respectively.

Metabolic studies

Whole-body energy metabolism was evaluated using a Comprehensive Lab Animal Monitoring System (CLAMS, Columbia Instruments). Animals were placed individually in chambers at ambient temperature (25°C) with 12-h light/dark cycles, VO2 is expressed as the volume of O2 consumed per kg0.75 weight per hour. VO2, carbon dioxide production, and the respiratory quotient were analysed during a 24-h time period. Continuous measurements were obtained over a 72-h time period. Mice were acclimated in the chambers for 2 days before the experiment to minimize the changes in housing environments.

For measurement of food consumption, 8-week-old *Cnot3*$^{ad-/-}$ mice and wild type controls (n = 4 each) were housed individually, consumption of foods and body weight were measured for 7 consecutive days. For measurement of rectal temperature, an

electronic thermistor (Model BAT-12) equipped with a rectal probe (RET-3, Physitemp) was used as described (Oike et al, 2005).

The high-fat diet study with 8-week-old *Cnot3*$^{ad-/-}$ mice and wild type controls (*n* = 4 each) was followed for a period of 12 weeks.

Magnetic Resonance Imaging

Magnetic resonance imaging with an 11.7 Tesla Magnetic Resonance scanner (Bruker, Billerica, MA, USA) was performed on 2% isofluorane-anaesthetized mice. The software Fiji (NIH, USA) was used for image analysis.

Histological analysis of tissue

After dissection, all tissues were fixed in 10% formaldehyde overnight. Paraffin-embedded sections were analyzed by haematoxylin and eosin staining. Morphometric analysis of adipose tissues from 500 cells per genotype was performed with Photoshop. For oil-red-O staining, the liver was frozen embedded.

Antibodies and reagents

Rabbit polyclonal antibodies against CNOT1, CNOT3, CNOT6L, CNOT7, and CNOT9 were as described (Morita et al, 2007). Mouse monoclonal antibody against CNOT3 was purchased from Abnova. Anti-Akt (#9272) and anti-phospho-Akt (Ser-473) (#9271) antibodies were purchased from Cell Signaling Technology. Anti-tubulin (T9026) and anti-GAPDH (#2118) were purchased from Sigma-Aldrich Co. and Cell Signaling Technology, respectively. Anti-perilipin (#9349S) was purchased from Cell Signaling Technology. Horseradish peroxidase-conjugated anti-rabbit IgG and anti-mouse IgG were from Amersham Biosciences. Human insulin was from Eli Lilly and Co.

Immunoblotting

Tissues were homogenized in lysis buffer (1% NP-40, 50mM Tris–HCl (pH 7.5), 150mM NaCl, 1mM EDTA, 1mM phenylmethylsulfonyl fluoride, 1mM NaF, 1mM Na3VO4) using a glass homogenizer and centrifuged for 10 min at 4℃. Protein concentrations were measured by the Bio-Rad protein assay. Proteins in the lysates were electrophoresed in SDS-polyacrylamide gel and then transferred onto Immobilon-P membranes (Millipore). Immunoblots were probed with the appropriate antibodies.

RNA analysis

For real-time PCR, total RNAs (1μg) were used for reverse transcription with oligo(dT) 12–18 primer (Invitrogen) using the SuperScript III First-Strand Synthesis System (Invitrogen). Real-time quantitative PCR reactions were carried out using SYBR Premix Ex Taq (Takara) and the ABI PRISM 7900HT Sequence Detection System (Applied Biosystems). 36B4 mRNA levels were used for normalization.

To measure mRNA stability, cells were treated with actinomycin D (5 mg/ml), and total RNAs were extracted at the indicated time points and subjected to qPCR analysis. The amount of reporter mRNAs was normalized to that of 36B4 mRNA.

Preparation of Primary MEF Cells

Primary MEF cells were isolated from E14.5 embryos. Embryos were removed and separated from maternal tissues and yolk sack and were finely minced, digested with 0.05% trypsin/ 1 mM EDTA for 30 min at 37°C, and centrifuged for 5 min at 1000g. The pellet was resuspended in culture medium before plating. Cells were cultured at 37 °C in high glucose DMEM containing 10% FBS and 100 units/ml

penicillin/streptomycin (Invitrogen). Experiments were performed at passage 2.

Adipocyte differentiation

White adipocyte differentiation was induced by treating confluent cells with medium containing 10% FBS, 0.5 mM methylisobutylxanthine, 1μMdexamethasone (DEX), 5 μg/ml insulin. Two days after induction, the medium was replaced with the maintenance medium containing 10% FBS, 5 μg/ml insulin. Brown adipocyte differentiation was induced by treating confluent cells with DMEM containing 10% FBS, 0.5mM isobutylmethylxanthine, 125 mM indomethacin, 2 mg/ml dexamethasone, 5 μg/ml insulin, 1 nM T3 and 0.5 mM rosiglitazone. Two days after induction, cells were switched to the maintenance medium containing 10% FBS, 5 μg/ml insulin, 1nM T3 and 0.5 mM rosiglitazone. Medium was renewed every 2 days.

Oil-red-O staining.

After 8 days of differentiation, cells were washed once in phosphate-buffered saline and fixed with 10% neutral buffered formalin solution (Sigma) for 15 min. The staining solution was prepared by dissolving 0.3 g oil-red-O (Sigma) in 100 ml of

isopropanol; before using, dilute six parts Oil Red-O stock with four parts distilled water, after 1 h at room temperature, the staining solution was filtered and added to dishes for 4 h. The staining solution was then removed, and cells were washed twice with distilled water.

Immunohistochemistry

Immunohistochemistry was performed using 4μm thick formalin-fixed, paraffin-embedded tissue sections. Briefly, slides deparaffinized in xylene were passed through graded alcohols and into PBS. Slides were then pretreated with 10 mM sodium citrate buffer, pH 6.0 kept at 121°C for 15 min using an autoclave (TOMY), followed by washing in PBS. Subsequent steps were performed at room temperature in a hydrated chamber. Slides were immersed in 3% H_2O_2 solution in absolute methanol at RT for 15 min to quench endogenous peroxidase activity. For macrophage staining: monoclonal rat anti-murine Mac2 (clone M3/38, Cedarlane) at 1:1000 was used. For apoptosis: monoclonal rabbit anti-murine Caspase3 antibody (Cell Signaling #9664) at 1:100 was used. For perilipin, monoclonal rabbit anti-perilipin (Cell Signaling #9349) at 1:100 was used. Slides were washed in PBS, and detected with with ***N***-Histofine®

Simple Stain Rat or Rabbit MAX PO (M) respectively. After further washing, brown immunoperoxidase staining was developed using a DAB chromogen (***N***-Histofine) and counterstained with hematoxylin (blue). Slides were examined and images were acquired with a fluorescence microscope (BZ-9000 All-in-one, KEYENCE).

Lipolysis assay

Epididymal fat pads from 4-5 mice were collected and digested in a digestion buffer (121 mM NaCl, 4.9 mM KCl, 1.2mM MgSO4, 0.33 mM CaCl2, 12 mM HEPES) containing dipase II (2.4 Uml-1), collagenese D (1.5 Uml-1), 3 mM glucose and 1 % fatty-acid-free BSA (Sigma). After digestion for 40 min at 37 °C with shaking, adipocytes were filtrated through nylon mesh and centrifuged at 200 g for 5 min. Floating adipocytes were collected and incubated in DMEM containing 10 % FBS with or without isoproterenol (1 mM) for 1.5 h at 37 °C. Glycerol released into the media was determined by using a free glycerol reagent (Sigma), the amounts of glycerol were normalized to the total protein content of the adipocytes by using a Pierce BCA Protein Assay reagent (Thermo Scientific).

Microarray analysis

Total RNAs were extracted with ISOGEN according to the manufacturer's protocol (Nippon Gene) and purified with an RNeasy Kit (Qiagen). cDNA and biotin-labelled cRNA were synthesized according to the protocols from Affymetrix. After fragmentation of cRNA, 20 mg biotin-labelled cRNA was hybridized to the GeneChip Mouse Genome 430 2.0 Array. To determine the average difference for each probe set, a global normalization method (Robust Multi-array Average) was used. Selected probe set IDs were converted to the manufacture's annotation. Enrichment of pathway was analyzed by Fisher's exact test followed by Bonferonni's correction. Microarray data of *aP2- nSrebp1c* mice (*Sr)* and *Pparg*$^{ldi/+}$ mice was obtained from the Gene Expression Omnibus (GEO) database, www.ncbi.nlm.nih.gov/geo (accession no. GSE9132).

Statistical analyses

All values represent mean values ± standard error of the mean (SEM). Differences between groups were examined for statistical significance using Student's t-test (two tailed distribution with two-sample equal variance). $P<0.05$ was considered significant throughout the study.

Results

Targeted deletion of *Cnot3* in mouse adipose tissues

To understand the role of *Cnot3* in adipose tissue, I generated mice in which *Cnot3* was knocked out specifically in adipose tissues (hereafter referred to as $Cnot3^{ad-/-}$). LoxP sites were introduced on either side of exons 2-9 of *Cnot3* to generate floxed *Cnot3* mice ($Cnot3^{lox/lox}$) (Morita et al., 2011), and these mice were crossed with Adipoq-cre mice that express Cre recombinase under the control of the mouse adiponectin (Adipoq) promoter (Eguchi et al., 2011) (Figure 3). Immunoblotting confirmed the absence of CNOT3 expression specifically in white adipose tissue (WAT) and interscapular brown adipose tissue (BAT) (Figure 4A), with unaltered CNOT3 expression in the liver, spleen and other tissues (Figure 4B).

Cnot3$^{ad-/-}$ mice exhibit lipodystrophy

$Cnot3^{ad-/-}$ mice were born at the expected Mendelian frequency, and there were no obvious morphological differences from control mice (Figure 5A). Although *Cnot3* haplodeficient mice were lean, $Cnot3^{ad-/-}$ mice were unexpectedly normal in size on a chow diet. Surprisingly, the total body weight of $Cnot3^{ad-/-}$ mice was slightly increased

compared with controls (Figure 5B). Dissection of *Cnot3*$^{ad-/-}$ mice revealed the following: (1) severely reduced epididymal WAT pads (eWAT) (Figure 6A) and subcutaneous, retroperitoneal, and mesenteric WAT pads (scWAT, rWAT, mWAT) (Figure 6B); and (2) markedly increased interscapular brown adipose tissue (BAT) (Figures 7A and B) that was pale in appearance. The sizes of other tissues in *Cnot3*$^{ad-/-}$ mice were not different from wild-type mice. Whole-body magnetic resonance imaging (MRI) analysis revealed a significant and global reduction in white adipose tissue mass, including subcutaneous, perigonadal, and mesenteric depots (Figures 7B and C). By contrast to the gross loss of WAT, cross-sectional examination of the interscapular region revealed enlarged BAT depots with increased lipid content (Figure 7A).

Comparison of *Cnot3*$^{ad-/-}$ mice and wild-type control mice by histological analysis using hematoxylin and eosin (H&E) staining revealed the following: (1) *Cnot3*$^{ad-/-}$ mice showed irregular sizes of white adipocytes and fibrotic WAT stroma (Figures 8A and B); (2) brown adipocytes in *Cnot3*$^{ad-/-}$ mice contained unilocular lipid deposition similar to that seen in immature white adipocytes (Figures 8C and D); and (3) increased lipid droplet accumulation was observed in hepatocytes from *Cnot3*$^{ad-/-}$ mice (Figures 8E and F). Oil-Red-O staining confirmed excessive hepatic lipid accumulation in *Cnot3*$^{ad-/-}$

mice compared with their wild-type littermates (Figures 8G and H). These observations suggested abnormal lipid accumulation in the liver and BAT of *Cnot3*$^{ad-/-}$ mice. Notably, these phenotypes of *Cnot3*$^{ad-/-}$ mice shared many of the features reported in human patients with Congenital Generalized Lipodystrophy (CGL) (Agarwal et al., 2006) and in mouse models of lipodystrophy, particularly *aP2-nSrebp1c* mice (*Sr*) (Shimomura et al. 1998).

To further confirm the lipodystrophic phenotype of *Cnot3*$^{ad-/-}$ mice, I compared the levels of circulating metabolic parameters between wild-type and *Cnot3*$^{ad-/-}$ mice. *Cnot3*$^{ad-/-}$ mice displayed typical metabolic sequelae of lipodystrophy, including hyperinsulinemia (Figure 9A), increased levels of circulating triglycerides (Figure 9B), hyperglycemia under fasting condition (Figure 9C), glucose intolerance (Figure 9D) and severe insulin resistance (Figure 9E).

Impaired thermogenic responses in *Cnot3*$^{ad-/-}$ mice

In rodents, one of the key mechanisms for heat generation and energy dissipation is thermogenesis in BAT (Seale et al., 2009). Given the hypertrophy and unilocular lipid

deposition in *Cnot3*$^{ad-/-}$ BAT, I hypothesized that BAT function was impaired. In the BAT of *Cnot3*$^{ad-/-}$ mice, expression of the BAT-specific uncoupling protein gene *Ucp1* was significantly decreased (Figures 10A and B). This change in BAT architecture suggested that, in an effort to increase their fat storage capabilities, *Cnot3*$^{ad-/-}$ mice transdifferentiate BAT to a more WAT-like phenotype. To address this possibility, the expression–of the white fat markers *HoxC8* and *Dpt* in BAT were analyzed using qRT-PCR (Sanchez-Gurmaches et al., 2012). Indeed, the BAT of *Cnot3*$^{ad-/-}$ mice showed higher expression of the white fat markers *HoxC8* and *Dpt* compared with wild-type mice (Figure 10C).

Because the BAT of *Cnot3*$^{ad-/-}$ mice appeared to be dysfunctional as a result of excess lipid accumulation, I assumed that thermogenesis in *Cnot3*$^{ad-/-}$ mice was impaired. Direct measurement of resting core body temperatures showed no significant differences between *Cnot3*$^{ad-/-}$ and wild-type mice (Figure 11A). To further assess thermogenic capacity and determine whether increased adaptive thermogenesis contributes to the enhanced energy expenditure in *Cnot3*$^{ad-/-}$ mice, we exposed 8-week-old *Cnot3*$^{ad-/-}$ and wild-type mice to a 4°C environment. Whereas wild-type mice maintained their body temperature at approximately 35.0°C during a 5 h cold

exposure, *Cnot3*$^{ad-/-}$ mice were intolerant to cold exposure and their body temperature dropped to 30°C by the end of a 5 h cold exposure (Figure 11B). These observations suggest that *Cnot3* deficiency impaired acute cold-induced thermogenesis.

Increased energy expenditure in *Cnot3*$^{ad-/-}$ mice

Because reduced adiposity indicates an energy balance disorder, it was necessary to address whether the reduced white adipose tissue size in *Cnot3*$^{ad-/-}$ mice resulted from increased energy expenditure. The energy available in food can be liberated in the body only as a result of oxidations, which ultimately depend on a supply of oxygen from the air, thus, a measurement of the oxygen uptake by the body is also a measure of energy expenditure (Durnin, 1984). Oxygen consumption (VO2) and carbon dioxide production (VCO2) occur during the oxidation of carbohydrate, protein, and fat. Heat production can be calculated from a measurement of VO2 and/or VCO2 (SparkNotes.com, 2014). I measured food intake and found that the rate of food intake per day was similar between *Cnot3*$^{ad-/-}$ and wild-type chow-fed mice (Figure 12). Next, whole-body energy metabolism was measured by monitoring oxygen consumption. Deletion of CNOT3 in adipose tissues resulted in increased oxygen consumption and

carbon dioxide production compared with control mice (Figures 13A, B, C and D). The respiratory exchange ratio (RER) did not show significant differences in fuel source usage (Figures 13E and F). These observations demonstrated that the deletion of CNOT3 in adipose tissues enhanced energy expenditure.

Because *Cnot3*$^{ad-/-}$ mice have smaller adipose stores (Figures 5 and 6), they assumed to exhibit symptoms of-cold stress even at 22°C. Indeed, *Ucp1* mRNA levels in the white adipose tissue of *Cnot3*$^{ad-/-}$ mice housed at 22°C were markedly elevated (Figure 14), suggesting exaggerated cold stress. Thus, the increased metabolic rate in *Cnot3*$^{ad-/-}$ mice might be a compensatory response to maintain normal body temperature in the absence of white adipose tissue. An increased resting energy expenditure (REE) also has been observed in human lipodystrophy syndromes (Cutler et al., 1991; Klein et al., 1992; Kosmiski et al., 2001). The increased energy expenditure in human lipodystrophy syndromes seems to be an adaptive response to an inability to store triacylglycerol fuel in a normal manner, which may represent a defense mechanism to protect non-adipose tissues from further lipid accumulation (Kosmiski et al., 2007).

Impaired lipolysis in the adipocytes of *Cnot3*$^{ad-/-}$ mice

Because an increased lipolysis rate results in reduced adiposity, I next performed an ex vivo lipolysis assay to examine whether the lipolysis rate was increased in the WAT of *Cnot3*$^{ad-/-}$ mice. Primary adipocytes from the epididymal fat pads of wild-type and *Cnot3*$^{ad-/-}$ mice were isolated, and their lipolysis rates were compared. Unexpectedly, primary adipocytes from *Cnot3*$^{ad-/-}$ mice showed severely impaired lipolysis (Figure 15). These observations suggested that the reduced adiposity in *Cnot3*$^{ad-/-}$ mice was not caused by increased lipolysis.

Adipose tissue inflammation and apoptosis in *Cnot3*$^{ad-/-}$ mice

The white adipose tissue of *Cnot3* $^{ad-/-}$ mice was unusual, having mononuclear cell infiltration and fibrotic stroma. The presence of inflammatory cell infiltration was further evaluated using quantitative RT-PCR. The expression of mRNAs corresponding to macrophage-related proteins were elevated in epididymal WAT and BAT from *Cnot3*$^{ad-/-}$ mice; these proteins included the chemokine MCP-1, the surface antigen Emr1 (recognized by an F4/80 antibody), and the macrophage transcription factor PU.1 (Figures 16A and B). Immunohistochemistry for MAC-2 (also known as galectin-3), a lectin expressed by activated macrophages that mediates macrophage phagocytic and

inflammatory responses, identified an increased number of MAC-2-positive macrophages in both epididymal WAT and BAT from *Cnot3* $^{ad-/-}$ mice compared with wild-type littermates. Macrophages in the surrounding remnants of lipid droplets of adipocytes were sometimes observed to form crown-like structures (CLSs) in the WAT of *Cnot3* $^{ad-/-}$ mice, whereas–these structures were almost absent from the WAT of wild-type mice (Figures 16C and D). Dramatically increased numbers of macrophages were also present and formed CLSs near adipocytes in the BAT of *Cnot3* $^{ad-/-}$ mice (Figures 16E and F).

The appearance of macrophages in the WAT and BAT of *Cnot3* $^{ad-/-}$ mice suggested the presence of ~~at~~ dead adipocytes. To confirm this, immunohistochemistry was performed using an antibody against perilipin, an essential protein that coats lipid droplets. The absence of perilipin staining indicates–dead or dying adipocytes. The results showed that the number of perilipin-negative cells in the epididymal WAT of *Cnot3*$^{ad-/-}$ mice was increased compared with littermate controls (Figures 17A and B), indicating that adipocytes were dying in the epididymal WAT of *Cnot3*$^{ad-/-}$ mice. Perilipin immunohistochemistry demonstrated that CLSs were selectively formed near perilipin-free adipocytes that lacked an intact plasma membrane.

I next tried to determine the causes of adipocyte death and the decrease in the size of white adipose tissue in *Cnot3*$^{ad-/-}$ mice. Immunohistochemical staining with anti-cleaved-caspase-3 antibodies revealed that the numbers of apoptotic cells in both WAT and BAT from *Cnot3*$^{ad-/-}$ mice were increased compared with control littermates (Figures 18A-D). The data suggested that adipocyte death was accelerated in the diminished WAT and hypertrophic BAT of *Cnot3*$^{ad-/-}$ mice. The massive apoptosis of metabolically active adipocytes clearly demonstrates that adipocyte destruction is the dominant pathological process involved in the loss of adipose tissue. It was hypothesized that increased apoptosis of peripheral adipocytes with impaired fat storage and lipid release may cause the lipodystrophic phenotype of *Cnot3* $^{ad-/-}$ mice. Microarray analysis was conducted to compare the gene expression profiles of epididymal fat pads in *Cnot3*$^{ad-/-}$ mice and their wild-type littermates. The results showed that pathways involved in apoptosis and inflammation were significantly up-regulated in *Cnot3*$^{ad-/-}$ mice (Table 1). The microarray data also revealed that expression of the SREBP/SREBF target gene was up-regulated. I focused on this gene because mice overexpressing the constitutively active *Srebp-1c* (one of the isoforms of *Srebp1)* transgene in adipocytes showed the same lipodystrophic phenotype (Shimomura et al.,

1998). Quantitative RT-PCR analysis confirmed that the expression level of *Srebp1* was significantly up-regulated in both WAT and BAT of *Cnot3*$^{ad-/-}$ mice (Figures 29A and B).

Common alterations in gene expression between *Cnot3*$^{ad-/-}$ mice and other lipodystrophy models

To further characterize the lipodystrophic phenotype in *Cnot3*$^{ad-/-}$ mice, compared the gene expression profiles of *Cnot3*$^{ad-/-}$ mice with those of two lipodystrophy model mice: *aP2- nSrebp1c* mice (*Sr*), which express the constitutively active *Srebp-1c* transgene in adipocytes, and *Pparg*$^{ldi/+}$ mice, which are generated by inserting the Tet activator (tTA) and a tTA-regulated *Flag-Pparg1* transgene into the *Pparg* gene. In total, 772, 722 and 751 transcripts were up-regulated >2.5-fold in the WAT of *Cnot3*$^{ad-/-}$, *Pparg*$^{ldi/+}$ and *Sr* epididymal fat pads, respectively, relative to their wild-type littermates (Figure 20). Of these, 100 genes were common among the three strains (Table 3). This substantial overlap in gene expression change may indicate widespread similarities in

the molecular basis of the lipodystrophic phenotype among the three strains, and those common genes may represent a typical signature of lipodystrophic fat.

Resistance to diet-induced obesity and enhanced energy expenditure in *Cnot3*$^{ad-/-}$ mice

Because *Cnot3*$^{ad-/-}$ mice exhibited reduced fat mass and increased energy expenditure under chow-fed condition, I next determined whether they would be resistant to weight gain when challenged with a high-fat diet. *Cnot3*$^{ad-/-}$ mice and wild-type littermates were fed a high-fat diet (HFD) for 3 months. During HFD feeding, *Cnot3*$^{ad-/-}$ mice gained significantly less weight than their wild-type littermates (Figure 21A and B). At the end of the HFD period, the net weight gains of wild-type and *Cnot3*$^{ad-/-}$ mice were 18.15 ± 0.68 g and 9.73 ± 1.39 g, respectively (Figure 21C). *Cnot3*$^{ad-/-}$ mice fed an HFD exhibited exacerbated lipodystrophy symptoms; their white adipose tissue size was dramatically reduced and brown adipose tissue was extremely hypertrophic compared with their wild-type littermates (Figures 22A and B). Whole-body magnetic resonance imaging (MRI) studies confirmed the exacerbated lipodystrophy in *Cnot3*$^{ad-/-}$ mice (Figure 23).

The observed resistance to obesity in *Cnot3*$^{ad-/-}$ mice suggested altered food intake or energy metabolism. Higher energy expenditure was observed by indirect calorimetry during both day and night cycles in *Cnot3*$^{ad-/-}$ mice (Figures 24A and B), even when their food intake was significantly increased (Figure 25A). The increase in oxygen consumption on the high-fat diet was approximately 17.4±0.5% and 17.1±0.6% during the light and dark phases, respectively. No differences were observed in the respiratory exchange ratio (RER) (Figures 24E and F). Despite increased energy expenditure, there was no difference in core body temperature between wild-type and *Cnot3*$^{ad-/-}$ mice (37.1±0.3°C and 37.5±0.2°C, respectively) (Figure 25B). These observations suggest that the *Cnot3*$^{ad-/-}$ mice were protected from obesity on a high-fat diet because of a significant increase in energy expenditure. The maintenance of normal body temperature despite increased energy expenditure indicated that because of the exacerbated lipodystrophy, increased energy expenditure is an adaptation to maintain body temperature in the absence of WAT.

Glucose and insulin tolerance tests were then performed in *Cnot3*$^{ad-/-}$ and wild-type mice. Surprisingly, in contrast to other models of lipodystrophy that exhibited exacerbated metabolic disorders when fed an HFD (Agarwal et al., 2006; Villena et al.,

2008), HFD-fed *Cnot3*$^{ad-/-}$ mice exhibited improved glucose tolerance and comparable insulin resistance compared with their wild-type littermates (Figures 26A and B). Morphological examination revealed that although the adipocytes of *Cnot3*$^{ad-/-}$ mice WAT were significantly smaller than those of wild-type mice (Figures 27A and B), lipid accumulation in the BAT and liver were at the same level compared with wild-type littermates (Figures 27C-F). Taken together, these observations indicate that although *Cnot3*$^{ad-/-}$ mice fed an HFD exhibited exacerbated lipodystrophy, ~~but~~ the metabolic consequences, such as glucose intolerance, insulin resistance and ectopic lipid accumulation, were not exacerbated compared with wild-type littermates.

Discussion

The CCR4-NOT complex contains at least 10 subunits. Aberrant regulation of several subunits of this complex, including CNOT1, CNOT3, CNOT6, CNOT6L, CNOT7, and CNOT8, has been implicated in the development of metabolic disorders (Morita et al., 2010; unpublished data). Whereas *Cnot3*$^{+/-}$ mice show defects in energy metabolism (Morita et al., 2010), there is no information about the effects of complete loss of *Cnot3* in metabolic tissues. To better understand the role of *Cnot3* in nutrient signaling and energy metabolism, I generated a mouse strain lacking *Cnot3* specifically in adipose tissue using the cre/loxP system. *Cnot3* deficiency in adipose tissues induces lipodystrophy, a rare disease characterized by a deficiency of adipose tissue.

Lipodystrophy is caused by multiple factors. Recent studies showed that lipodystrophy can result from either the suppression or the overexpression of various genes; several lipodystrophic mouse models have been generated by disrupting transcription factor-coding genes, including peroxisome proliferator activated receptor (PPAR)γ (He W et al., 2003), sterol regulatory element binding protein (SREBP)1c (Shimomura I et al., 1998), and CCAAT/enhancer-binding proteins (C/EBPs) (Chatterjee R et al., 2010). In this study, I provide evidence that impairment of

CCR4-NOT deadenylase complex, another regulator of gene expression, induces a lipodystrophic phenotype. I further provide evidence that *Cnot3* deficiency caused massive inflammation and apoptosis in adipose tissues, which together at least partially account for the lipodystrophic phenotype. Furthermore, *Cnot3* might target mRNAs related to lipodystrophy, such as *Srebp1* mRNA, so that CCR4-NOT can deadenylate these mRNAs.

Mice showing haploinsufficiency of the *Cnot3* in whole body are lean with decreased adiposity and have increased metabolic rates and enhanced glucose tolerance (Morita et al., 2010). Deletion of *Cnot3* in an adipose tissue-specific manner caused massive fat loss, but these mice are not lean and show insulin resistance and impaired glucose tolerance, suggesting that the balance of *Cnot3* expression in adipose tissue has a very important role in maintaining adipocyte viability and whole body metabolism.

Lipodystrophy is commonly ascribed to defective adipocyte differentiation (Garg A et al., 2004; Capeau J et al., 2005; Moitra J et al., 1998; Shimomura I et al., 1998; Peterfy M et al., 2001). Because the Cre transgenic mice I used to generate *Cnot3*$^{ad-/-}$ mice express Cre recombinase only in mature adipocytes, the differentiation of

adipocytes should not have been impaired; therefor, the fat loss and subsequent progressive lipodystrophy in *Cnot3*$^{ad-/-}$ mice are not due to defective adipocyte differentiation.

The phenotype of *Cnot3*$^{ad-/-}$ mice is similar to that of the established lipodystrophy model, *aP2-nSREBP-1c* transgenic mice (Shimomura et al. 1998) , which have the unique combination of hypoplastic WAT and hypertrophic BAT. These traits and their metabolic consequences resemble the HIV-associated lipodystrophy of patients under combined antiretroviral therapy (cART) against HIV infection, in which peripheral fat depots degenerate and visceral, neck (buffalo hump) and breast fat depots expand (Carr A et al., 1998; Grinspoon et al., 2005). Our results demonstrate that *Cnot3*$^{ad-/-}$ mice constitute an interesting experimental model to understand the molecular basis of lipodystrophy induced by cART in humans. Further studies are required to addres the relationship between hypoplastic WAT and hypertrophic BAT. BAT-specific KO of *Cnot3* would provide more conclusive evidence for the role of *Cnot3* in this tissue.

Cnot3$^{ad-/-}$ mice exhibited severe insulin resistance (Figure 10E). Alterations in adipocyte functions, such as the capacity to store lipids and secrete adipokines, and

ectopic accumulation of lipids in tissues other than adipose tissue are considered to be major causes of the development of insulin resistance (Shulman, 2000; Villena et al., 2008). In addition, hyperlipidemia and the appearance of insulin resistance are often associated with the activation of inflammatory pathways (Wellen et al., 2005). Therefore, altered inflammatory pathways in *Cnot3*$^{ad-/-}$ mice may contribute to their insulin resistance.

Cnot3$^{ad-/-}$ mice also exhibited increased energy expenditure. This finding is consistent with other reports of increased resting energy expenditure (REE) in humans with lipodystrophy syndromes (Cutler et al., 1991; Klein et al., 1992; Kosmiski et al., 2001). Acute cold-induced thermogenesis was impaired in *Cnot3*$^{ad-/-}$ mice, suggesting that the increased metabolic rate of *Cnot3*$^{ad-/-}$ mice may not be a direct consequence of *Cnot3* deficiency but rather a compensatory response to maintain normal body temperature in the absence of white adipose tissue.

Furthermore, deletion of *Cnot3* in adipose tissue prevents the body weight gain and adipose tissue accumulation that are normally associated with high-fat diets. Unlike other models of lipodystrophy that show exacerbated metabolic disorders under high-fat

feeding conditions (Agarwal et al., 2006; Villena et al., 2008), *Cnot3*$^{ad-/-}$ mice fed an HFD exhibited exacerbated lipodystrophy, but the metabolic consequences of this lipodystrophy, such as glucose intolerance, insulin resistance and ectopic lipid accumulation, were not exacerbated compared with wild-type littermates. It was hypothesized that the increased energy expenditure might be an adaptive response to an inability to store triacylglycerol fuel in a normal manner, which may represent a defense mechanism to protect non-adipose tissues from further lipid accumulation (Kosmiski et al., 2007). The mechanism underlying this phenotype was not investigated further, but deserves additional studies.

In conclusion, this study describes the lipodystrophic phenotype caused by the deletion of *Cnot3* specifically in adipose tissue. Microarray analysis revealed that a reduction in CNOT3 levels specifically in adipose tissue affects the expression of mRNAs that encode proteins important for lipid metabolism, inflammation, and apoptosis. Thus, the *Cnot3*$^{ad-/-}$ mice may be a novel valuable animal model of partial lipodystrophy and insulin resistance in humans. Overall, this study links CCR4-NOT complex function to lipodystrophy syndrome for the first time, and our findings raise

the intriguing possibility that CNOT3 and the CCR4-NOT deadenylase complex can serve as therapeutic targets to treat lipodystrophy and its associated metabolic disorders.

References

Aslam A., Mittal S., Koch F., Andrau J. C., Winkler G. S. (2009) The Ccr4-Not deadenylase subunits CNOT7 and CNOT8 have overlapping roles and modulate cell proliferation. *Mol. Biol. Cell* 20: 3840–3850.

Agarwal A. K., Garg A. (2006) Genetic basis of lipodystrophies and management of metabolic complications. *Annu. Rev. Med.* 57: 297–310.

Bai Y., Salvadore C., Chiang Y. C., Collart M. A., Liu H. Y., Denis C. L. (1999) The CCR4 and CAF1 proteins of the CCR4–NOT complex are physically and functionally separated from NOT2, NOT4, and NOT5. *Mol. Cell Biol.* 19: 6642–6651.

Berthet C., Morera A. M., Asensio M. J., Chauvin M. A., Morel A. P., Dijoud F., Magaut J. P., Durand P., Rouault J. P. (2004) CCR4-associated factor CAF1 is an essential factor for spermatogenesis. *Mol. Cell Biol.* 24: 5808–5820.

Capeau J., Magré J., Lascols O., Caron M., Béréziat V., Vigouroux C., Bastard J. P. (2005) Diseases of adipose tissue: genetic and acquired lipodystrophies. *Biochem. Soc. Trans.* 33: 1073–1077.

Caron-Debarle M., Lagathu C., Boccara F., Vigouroux C., Capeau J. (2010) HIV-associated lipodystrophy: from fat injury to premature aging. *Trends Mol. Med.* 16: 218–229.

Carr A., Samaras K., Burton S., Law M., Freund J., Chisholm D. J. (1998) A syndrome of peripheral lipodystrophy, hyperlipidaemia and insulin resistance in patients receiving HIV protease inhibitors. *AIDS.* 12: F51–F58.

Chatterjee R., Bhattacharya P., Gavrilova O., Glass K., Moitra J., Myakishev M., Pack S., Jou W., Feigenbaum L., Eckhaus M., and Vinson C. (2010) Suppression of the C/EBP family of transcription factors in adipose tissue causes lipodystrophy. *J Molecular Endocrinology.* 46(3): 175-192.

Chen C., Ito, K., Takahashi A., Wang G., Suzuki T., Nakazawa T., Yamamoto T., Yokoyama K. (2010) Distinct expression patterns of the subunits of the CCR4-NOT deadenylase complex during neural development. *Biochem. Biophys. Res. Commun.* 410: 360–364.

Collart M. A. (2003) Global control of gene expression in yeast by the Ccr4-Not complex. *Gene* 313: 106.

Collart M. A., Timmers H. T (2004) The eukaryotic Ccr4-not complex: a regulatory platform integrating mRNA metabolism with cellular signaling pathways? *Prog. Nucleic Acid Res. Mol. Biol.* 77: 289–322.

Collart M. A., Panasenko O. O. (2012) The CCR4-not complex. *Gene* 492: 42–53.

Consortium A. G. O. (2008) The Gene Ontology project in 2008. *Nucleic Acids Research* 36: D440–444.

Cutler D. L., Kaufmann S., Freidenberg G. R. (1991) Insulin-resistant diabetes mellitus and hypermetabolism in mandibuloacral dysplasia: a newly recognized form of partial lipodystrophy. *J. Clin. Endocrinol. Metab*. 73: 1056 – 61.

Dupressoir A., Morel A. G., Barbot W., Loirreau P., Corbo L., Heidmann T. (2001) Identification of four families of yCCR4- and Mg^{2+}-dependent endonuclease-related proteins in higher eukaryotes, and characterization of orthologs of yCCR4 with conserved leucine-rich repeat essential for hCAF1/hPOP2 binding. *BMC Genomics* 2: 9S.

Durnin J. (1984) Measuring impact on physical activity and physical fitness: Chapter 8 in Methods for the evaluation of the impact of food and nutrition programmes. Edited

by David E. Sahn, Richard Lockwood, and Nevin S. Scrimshaw. United Nations University Press.

Eguchi J., Wang X., Yu S., Kershaw E. E., Chiu, P. C., Dushay J., Estall J. L., Klein U., Maratos-Flier E., Rosen E. D. (2010) Transcriptional control of adipose lipid handling by IRF4. *Cell Metab*. 13: 249–259.

Fisher F. M., Kleiner S., Douris N., Fox E. C., Mepani R. J., Verdeguer F., Wu J., Kharitonenkov A., Flier J. S., Maratos-Flier E., Spiegelman B. M. (2012) FGF21 regulates PGC-1a and browning of white adipose tissues in adaptive thermogenesis. *Genes Dev.* 26: 271–281.

Feldmann H. M., Golozoubova V., Cannon, B., Nedergaard J. (2009) UCP1 ablation induces obesity and abolishes diet-induced thermogenesis in mice exempt from thermal stress by living at thermoneutrality. *Cell Metab.* 9: 203–209.

Frayn K. N. (2002) Adipose tissue as a buffer for daily lipid flux. *Diabetologia.* 45: 12010210.

Garg A. (2000) Lipodystrophies. *Am. J. Med. Sci.* 108: 143–152.

Garg A. (2004) Acquired and inherited lipodystrophies. *N. Engl. J. Med.* 350: 1220–

1234.

Garg A. (2006) Adipose tissue dysfunction in obesity and lipodystrophy. *Clin. Cornerstone* 8(Suppl4): S7–S13.

Garg A., Agarwal A. K. (2009) Lipodystrophies: disorders of adipose tissue biology. *BBA Mol. Cell Biol. L*. 1791: 507–513.

Garg A. (2010) Lipodystrophies: genetic and acquired body fat disorders. *J. Clin. Endocrinol Metab*. 96: 3313–3325

Grinspoon S., Carr A. (2005) Cardiovascular risk and body-fat abnormalities in HIV-infected adults. *N. Engl. J. Med.* 352, 48–62.

Gupta R. K., Arany Z., Seale P., Mepani R. J., Ye L. (2010) Transcriptional control of preadipocyte determination by Zfp423. *Nature* 464: 619–623.

He W., Barak Y., Hevener A., Olson P., Liao D., Le J., Nelson M., Ong E., Olefsky J.M., Evans R.M. (2003) Adipose-specific peroxisome proliferator-activated receptor gamma knockout causes insulin resistance in fat and liver but not in muscle. *PNAS.* 100: 15712–15717.

Hegele R. A., Joy T. R., Al-Attar S. A., and Rutt B. K. (2007) Thematic review series:

adipocyte biology. lipodystrophies: windows on adipose biology and metabolism. *J. Lipid Res*. 48 : 1433–1444.

Herrero L., Shapiro H., Nayer A., Lee J., Shoelson S. E. (2010) Inflammation and adipose tissue macrophages in lipodystrophic mice. *PNAS*. 107: 240–245.

Kershaw E. E., Flier J. S. (2004) Adipose tissue as an endocrine organ. *J. Clin. Endocrinol. Metab.* 89: 2548–2556.

Klein S., Jahoor F., Wolfe R. R., Stuart C. A. (1992) Generalized lipodystrophy: in vivo evidence for hypermetabolism and insulin-resistant lipid, glucose and amino acid kinetics. *Metabolism*41: 893– 896.

Kosmiski L. A., Kuritzkes D. R., Lichtenstein K. A. (2001) Fat distribution and metabolic changes are strongly correlated and energy expenditure is increased in the HIV lipodystrophy syndrome. *AIDS* 15: 1993–2000.

Kosmiski L. A., Kuritzkes D. R., Sharp T. A., Hamilton J. T., Lichtenstein K. A., Mosca C. L., Grunwald G. K., Eckel R. H., Hill J. O. (2003) Total energy expenditure and carbohydrate oxidation are increased in the human immunodeficiency virus lipodystrophy syndrome. *Metabolism* 52: 620–625.

Liisberg Aune U., Ruiz L., Kajimura S. (2013) Isolation and differentiation of stromal vascular cells to beige/brite cells. *J. Visual. Exp.* E50191.

Liu H. Y., Badarinarayana V., Audino D. C., Rappsilber J., Mann M., Denis C. L., (1998) The NOT proteins are part of the CCR4 transcriptional complex and affect gene expression both positively and negatively. *EMBO J*. 17: 1096–1006.

Marshall B. A., Ren J. M., Johnson D. W., Gibbs E. M., Lillquist J. S. (1993) Germline manipulation of glucose homeostasis via alteration of glucose transporter levels in skeletal muscle. *J. Biol. Chem*. 268: 18442–18445.

Moitra J., Mason M. M., Olive M., Krylov D., Gavrilova O., Marcus-Samuels B., Feigenbaum L., Lee E., Aoyama T., Eckhaus M. (1998) *Genes Dev*. 12: 3168–318.

Morita M., Oike Y., Nagashima T., Kadomatsu T., Tabata M. (2010) Obesity resistance and increased hepatic expression of catabolism-related mRNAs in *Cnot3*$^{+/-}$ mice. *EMBO J.* 30: 4678–4691.

Morita M., Suzuki T., Nakamura T., Yokoyama K., Miyasaka T., and Yamamoto T. (2007) Depletion of mammalian CCR4b deadenylase triggers elevation of the p27Kip1 mRNA level and impairs cell growth. *Mol. Cell. Biol.* 27: 4980–4990.

Mallewa J. E., Wilkins E., Vilar J., Mallewa M., Doran D., Back D., Pirmohamed M. (2008) HIV-associated lipodystrophy: a review of underlying mechanisms and therapeutic options. *J. Antimicrob. Chemother*. 62: 648–660.

Nagy G. S., Tsiodras S., Martin L. D., Avihingsanon A., Gavrila A., Hsu W. C., Karchmer A. W., Mantzoros C. S. (2003) Human immunodeficiency virus type 1-related lipoatrophy and lipohypertrophy are associated with serum concentrations of leptin. *Clin. Infect. Dis.* 36: 795–802.

Nakamura T., Yao R., Ogawa T., Suzuki T., Ito C., Tsunekawa N., Inoue K., Ajima R., Miyasaka T., Yoshida Y. (2004) Oligo-astheno-teratozoospermia in mice lacking Cnot7, a regulator of retinoid X receptor beta. *Nature Gene.* 36: 528–533.

Nakashima K., Noda T., Yamamoto T., Noda M. (2007) Cnot7-null mice exhibit high bone mass phenotype and modulation of BMP actions. *J. Bone Miner. Res.* 22: 1217–1223.

Neely G. G., Kuba K., Cammarato A., Isobe K., Amann S., Zhang L., Murata M., Elmen L., Gupta V., Arora S., Sarangi R., Dan D., Fujisawa S., Usami T., Xia C. P., Keene A. C., Alayari N. N., Yamakawa H., Elling U., Berger C. (2010) A global in vivo

Drosophila RNAi screen identifies NOT3 as a conserved regulator of heart function. *Cell* 141042–153.

Ohno H., Shinoda K., Ohyama K., Sharp LZ., Kajimura S. (2013) EHMT1 controls brown adipose cell fate and thermogenesis through the PRDM16 complex. *Nature* 504: 163–167.

Peterfy M., Phan J., Xu P., Reue K. (2001) Lipodystrophy in the fld mouse results from mutation of a new gene encoding a nuclear protein, lipin. *Nat. Gene.* 27: 121024.

Phan J., Reue K. (2005) Lipin, a lipodystrophy and obesity gene. *Cell Metab.* 1: 73–83.

Sanchez-Gurmaches J., Hung C. M., Sparks C. A., Tang Y., Li H., Guertin D. A. (2012) *PTEN* loss in the Myf5 lineage redistributes body fat and reveals subsets of white adipocytes that arise from Myf5 precursors. *Cell Metab.* 16: 348–362.

Savage D. B. (2009) Mouse models of inherited lipodystrophy. *Dis. Model. Mech.* 2: 554–562.

Seale P, Lazar M. A. (2009) Brown Fat in Humans: Turning up the Heat on Obesity. *Diabetes.* Jul; 58(7):1482-4.

Shimomura I., Hammer R. E., Richardson J. A., Ikemoto S., Bashmakov Y., Goldstein J. L., Brown M. S. (1998) Insulin resistance and diabetes mellitus in transgenic mice expressing nuclear SREBP-1c in adipose tissue: model for congenital generalized lipodystrophy. *Genes Dev.* 12: 3182–3194.

Shimomura I., Hammer R. E., Ikemoto S., Brown M. S., Goldstein, J. L. (1999) Leptin reverses insulin resistance and diabetes mellitus in mice with congenital lipodystrophy. *Nature* 401: 73–76.

Shimomura I., Matsuda M., Hammer R. E., Bashmakov Y., Brown M. S., Goldstein J. L. (2000) Decreased IRS-2 and increased SREBP-1c lead to mixed insulin resistance and sensitivity in livers of lipodystrophic and ob/ob mice. *Mol. Cell* 6: 77–86.

Shulman G. I. (2000) Cellular mechanisms of insulin resistance. *J. Clin. Invest.* 106: 171076.

SparkNotes Editors. (2014) "Sparknote on nutritional assessment and profiling: Anthropometric." SparkNotes.com. SparkNotes LLC. n.d.. Web.

Strissel K. J., Stancheva Z., Miyoshi H., Perfield J. W. II., DeFuria J., Jick Z. (2007) Adipocyte death, adipose tissue remodeling, and obesity complications. *Diabetes* 56, 2910–2918.

Strickland L. R., Guo F., Lok K., Garvey W. T. (2013) Type 2 diabetes with partial lipodystrophy of the limbs: a new lipodystrophy phenotype. *Comment in Diabetes Care.* 36: 2142–5.

Sutinen J., Yki-Järvinen H. (2007) Increased resting energy expenditure, fat oxidation, and food intake in patients with highly active antiretroviral therapy-associated lipodystrophy. *Am. J. Physiol. Endocrinol. Metab*. 292: E687–E692.

Kim S., Huang L. W., Snow K. J., Ablamunits V., Hasham M. G., Young T. H., Paulk A. C., Richardson J. E., Affourtit J. P., Shalom-Barak T., Bult C. J., Barak Y. (2007) A mouse model of conditional lipodystrophy. *PNAS.* 104: 16627–16632.

Temme C., Simonelig M., Wahle E. (2014) Deadenylation of mRNA by the CCR4-NOT complex in Drosophila: molecular and developmental aspects. *Front. Gene.* 5: 143.

Tucker M., Valencia-Sanchez M. A., Staples R. R., Chen J., Denis C. L., Parker R. (2001) The transcription factor associated Ccr4 and Caf1 proteins are components of the major cytoplasmic mRNA deadenylase in saccharomyces cerevisiae. *Cell* 104: 377–386.

Villena J. A., Choi C. S., Wang Y., Kim S., Hwang Y. H., Kim Y. B., Cline G., Shulman G. I., Sul H. S. (2008) Pref-1 confers resistance to diet induced obesity but exacerbates insulin resistance in mice. a new model of partial lipodystrophy. *Diabetes* 57: 3258–3266.

Vergnes L., Beigneux A.P., Davis R., Watkins S.M., Young S. G., Reue K. (2006) Agpat6 deficiency causes subdermal lipodystrophy and resistance to obesity. *J. Lipid Res.* 47: 745–754.

Washio-Oikawa K., Nakamura T., Usui M., Yoneda M., Ezura Y., Ishikawa I., Nakashima K., Noda T., Yamamoto T., Noda M. (2007) Cnot7-null mice exhibit high bone mass phenotype and modulation of BMP actions. *J. Bone Miner. Res.* 22: 1217–1223.

Watanabe C., Morita M., Hayata T., Nakamoto T., Kikuguchi C., Li X., Kobayashi Y., Takahashi N., Notomi T., Moriyama K. (2014) Stability of mRNA influences osteoporotic bone mass via CNOT3. *PNAS.* 101: 2692–2697.

Wellen K. E., Hotamisligil G. S. (2005) Inflammation, stress, and diabetes. *J. Clin. Invest.* 105: 1010–1019.

Winkler G. S., Balacco D. L. (2013) Heterogeneity and complexity within the nuclease module of the Ccr4-Not complex. *Front. Gene.* 4: 296.

Yamashita A., Chang T. C., Yamashita Y., Zhu W., Zhong Z., Chen C. Y., Shyu A. B. (2005) Concerted action of poly(A) nucleases and decapping enzyme in mammalian mRNA turnover. *Nat. Struct. Mol. Biol.* 12: 1054–1063.

Acknowledgments

I give the greatest gratitude to my supervisors Professor Tadashi Yamamoto and Professor Yuji Yamanashi for their continual guidance, words of wisdom, and friendship. They have been by my side in every difficult moment and provided me with much more support and understanding than one could possibly expect from a PhD supervisor. During my PhD dissertation study, I have learned a lot from them, not only scientifically, but also personally.

I acknowledge Dr. Toru Suzuki very much for friendly reviewing this thesis. His constructive suggestions really helped me to improve this thesis in many aspects.

Sincere thanks to Dr. Masahiro Morita, Dr. Akinori Takahashi, Dr. Kentaro Ito, Mr. Shin-ichi Ogawa, Dr. Naosuke Hoshina, Dr. Taku Kureha for their helpful discussions and technical advices.

I am grateful to for Associate Professor Ohsugi Miho, Dr. Noriko Tokai-Nishizumi, Dr. June Goto-Nakamura, Dr. Naoki Oshimori for kind encouragement at the beginning year of my PhD course.

The great appreciation to Professor Kajimura Shingo at the University of California, Assistant professor Takahisa Nakamura at Cincinnati Children's Hospital Medical Center for valuable suggestions and helpful discussions, enriched my knowledge.

I thank all my past and present members in the Yamamoto laboratory, who were always there for help, suggestions and fruitful discussions. Thanks Ms. Yuki Sakaizumi and Ms. Kaori Yamashiro for the help on daily events. Thanks Chisato Kikuguchi, Miho Tokumasu, for sharing their pleasures in daily life. I appreciate my dear friends Ms. Chihiro Arasaki, Ms. Qiong Huang, Dr. Shaofang Wang, Dr. Shun-Jen Yang for their kind friendship and the help in many aspects.

To my father Mr. Peiguo Li and mother Ms. Wanmei Wang for their endless love and encouragement. Without their strong support in both spirit and economy, I have no encouragement to go abroad and to pursue what I want. Special thanks to my sister Ms. Fujuan Li, for kind encouragement and strong personally support and for sharing parts of my happiness and toughness at the beginning year of my PhD course.

To my beloved husband Zhenghong Gao to whom this thesis is dedicated. Hong has been there for me all the time, with a dedication that is beyond any words.

Lastly, I would like to thank Japan for being such a great country receiving me with wide opening arms.

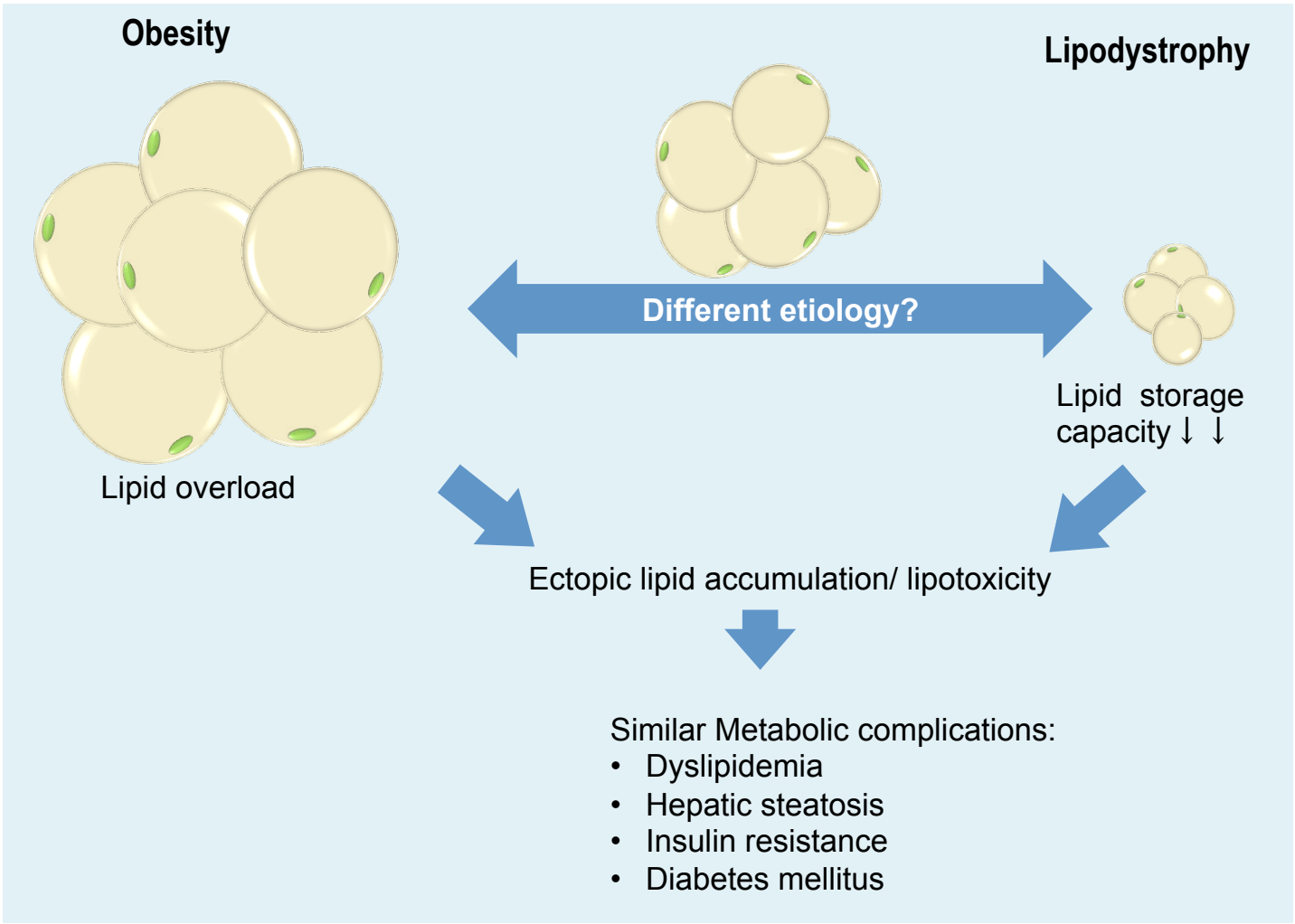

Figure 1. Schematic illustration of lipodystrophy. Lipodystrophy and obesity are caused by different etiology but accompanied by similar metabolic consequences including dyslipidemia, hepatic steatosis, severe insulin resistance, and diabetes mellitus.

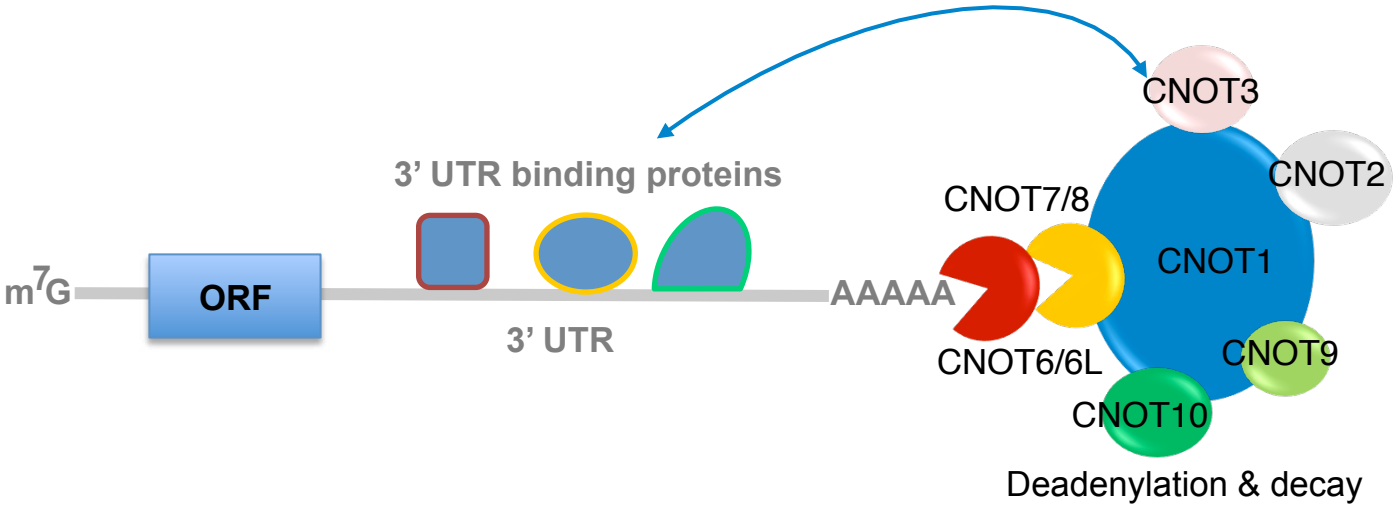

Figure 2. Schematic illustration of the CCR4-NOT complex and the role of CNOT3. The CCR4–NOT complex is a major deadenylase that regulates mRNA degradation by catalyzing the removal of mRNA poly(A) tails. The CNOT3 non-catalytic component of the mammalian CCR4-NOT complex is involved in recruitment of the CCR4-NOT to the 3' end of specific mRNAs.

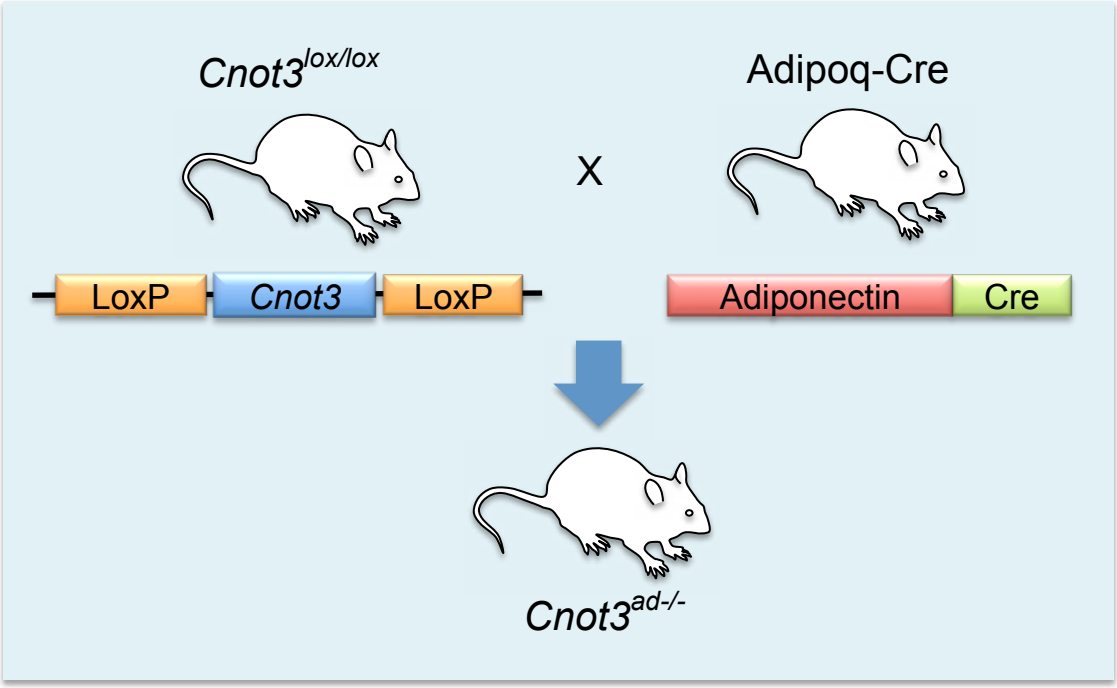

Figure 3. Targeted disruption of the *Cnot3* gene in adipose tissues.

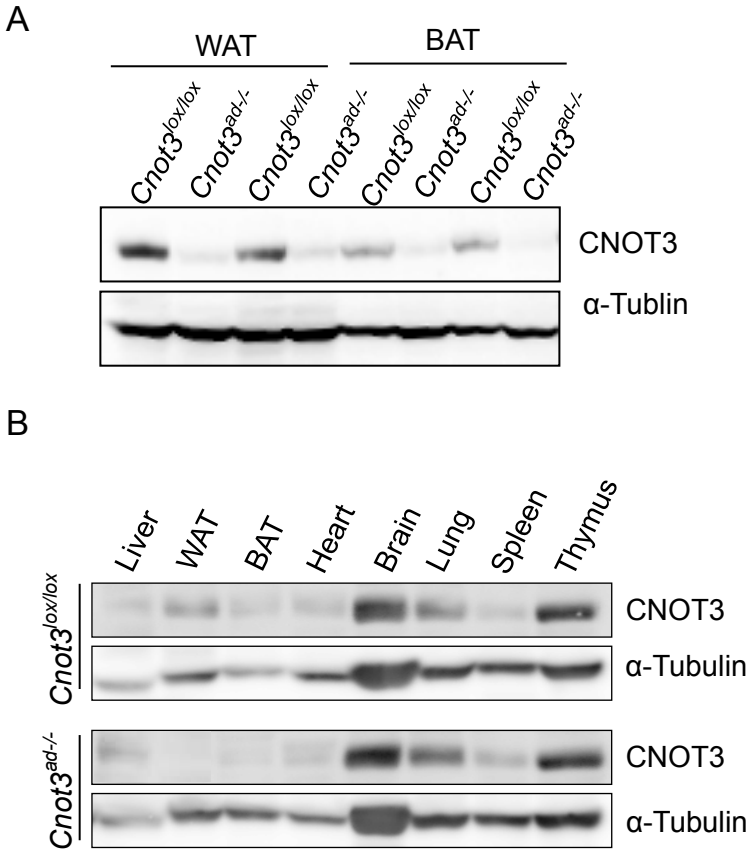

Figure 4.(A) Western blot of CNOT3 and α-Tubulin protein by western blot in white adipose tissue (WAT) and brown adipose tissue (BAT) of *Cnot3*$^{lox/lox}$ control and *Cnot3*$^{ad-/-}$ mice. (B) Tissue distribution of CNOT3 protein by western blot in *Cnot3*$^{lox/lox}$ control and *Cnot3*$^{ad-/-}$ mice. .

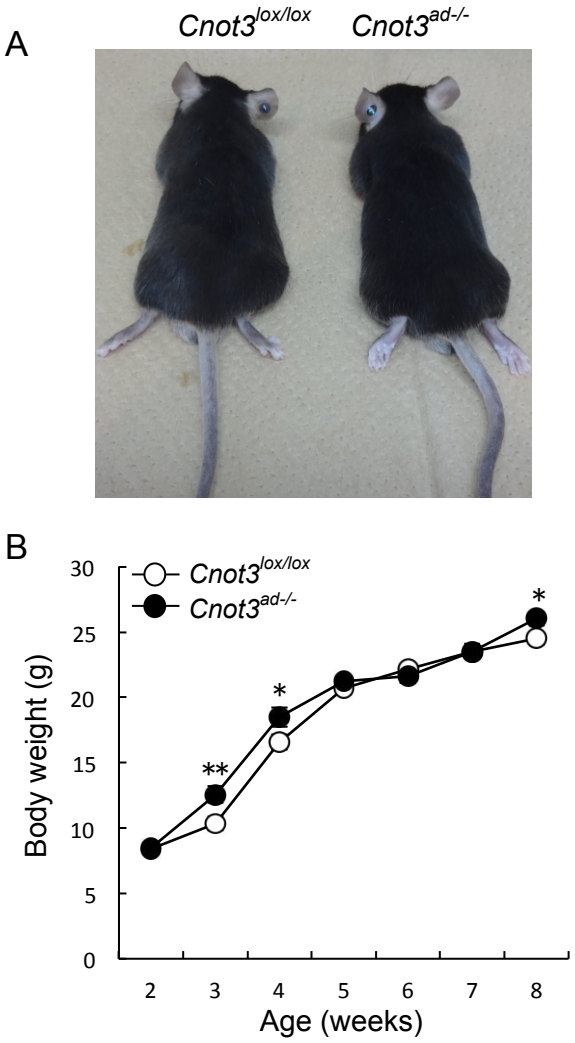

Figure 5. There were no obvious morphological differences in *Cnot3*$^{ad-/-}$ mice. (A) Gross appearance of 8-week-old *Cnot3*$^{ad-/-}$ mice and their wild-type littermates on ND feeding. (B) Growth curve of *Cnot3*$^{ad-/-}$ mice and their wild-type littermates from 2 to 8 weeks after birth. *n*=10 for each genotype. Results expressed as mean ± SEM, *p < 0.05, * * p < 0.01, * * * p < 0.001.

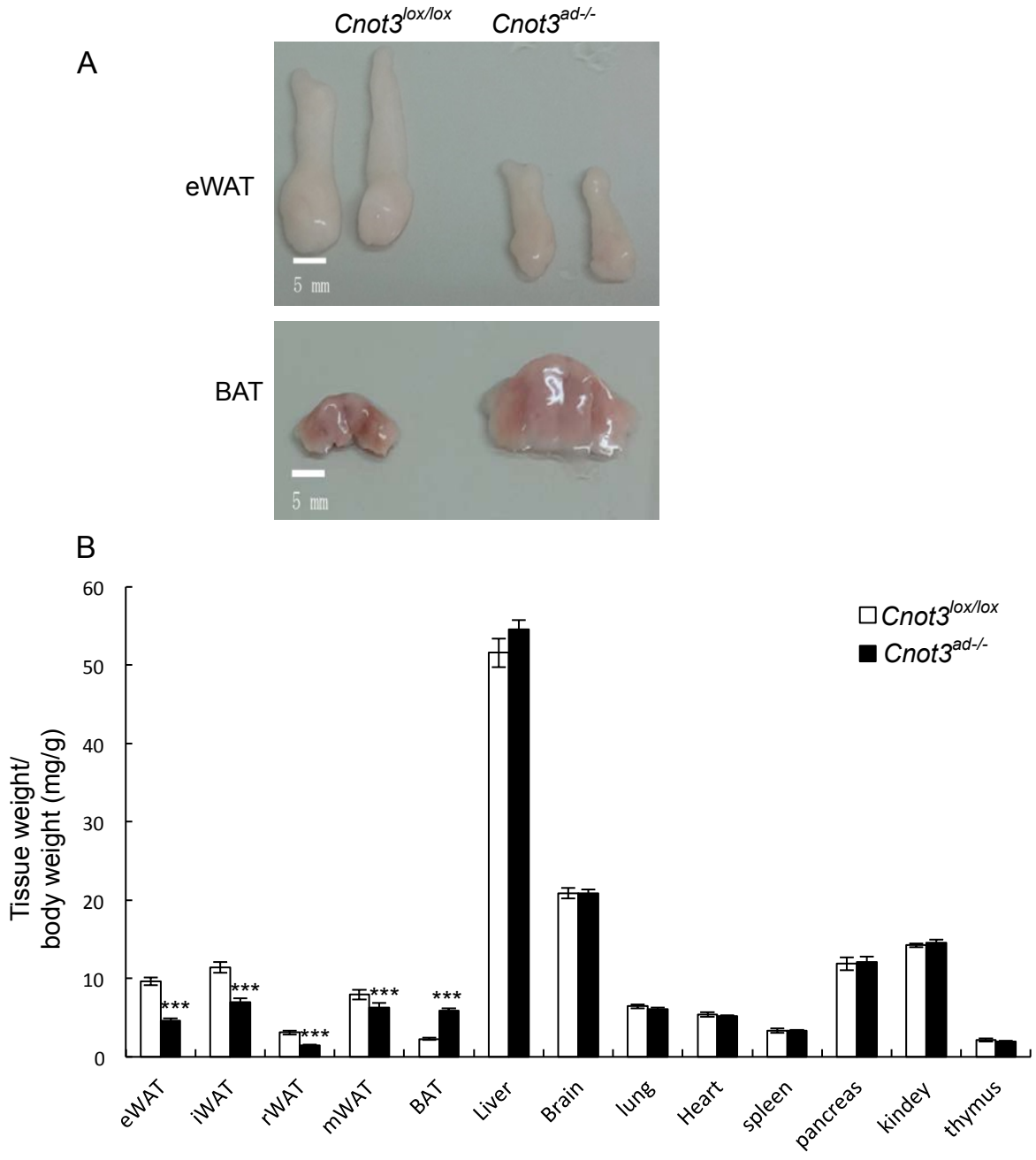

Figure 6. Severely reduced size of WAT and markedly enlarged BAT.(A) Fat pads morphology of wild-type and *Cnot3*$^{ad-/-}$ mice. (B) The relative weight of the indicated organs. The weight of the organ was normalized to body weight. *n*=8-10 for each genotype. Results expressed as mean ± SEM, *p < 0.05, * * p < 0.01, * * * p < 0.001.

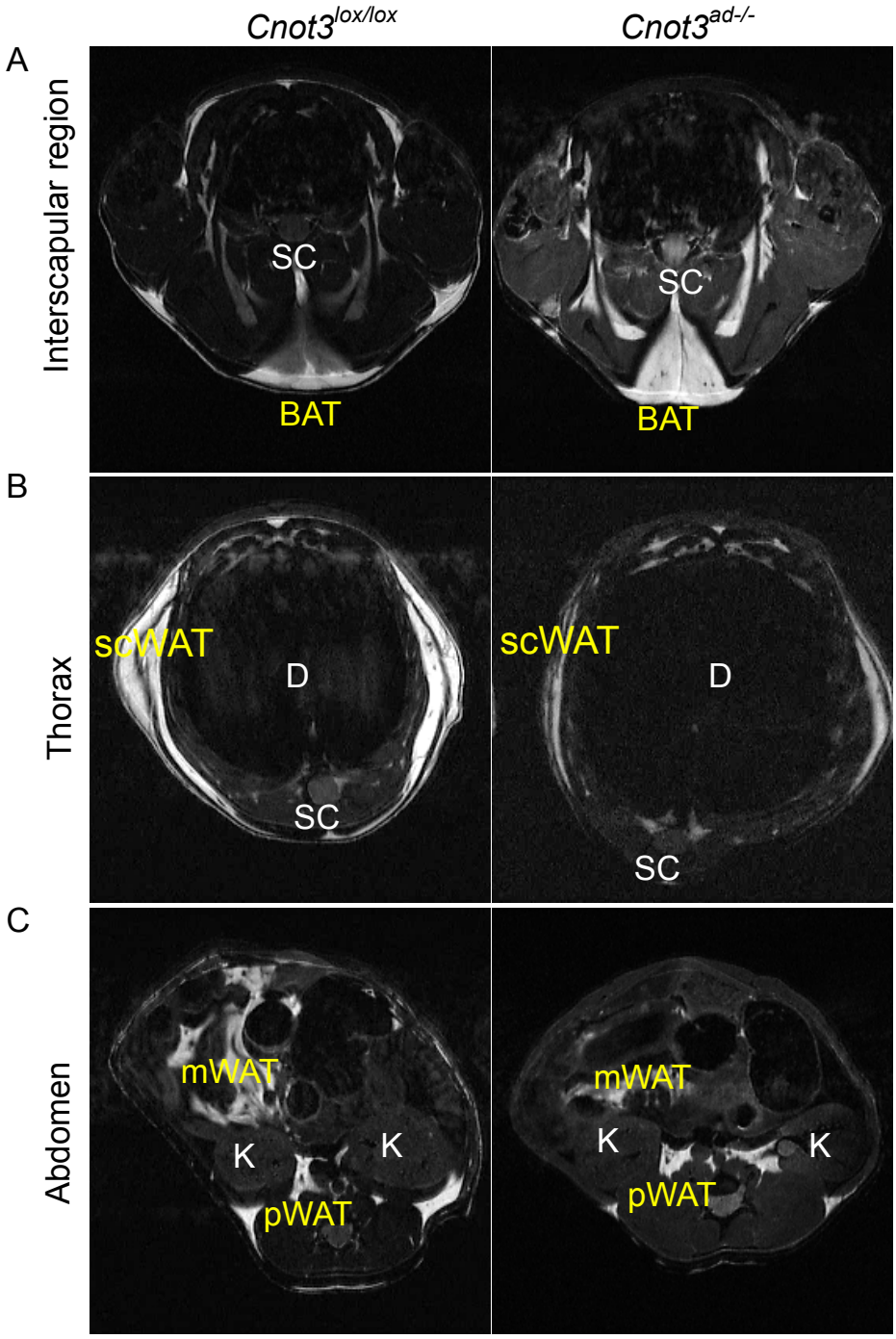

Figure 7. MRI imaging of wild-type (left) and *Cnot3*$^{ad-/-}$ (right) mice at 8 weeks on ND feeding. Cross-section at the level of the interscapular region (A), thorax (B) and abdomen (C). D, diaphragm; scWAT, subcutaneous WAT; mWAT, mesenteric WAT; pWAT, retroperitoneal fat; BAT , Interscapular BAT; SC, spinal cord;. K, kidney.

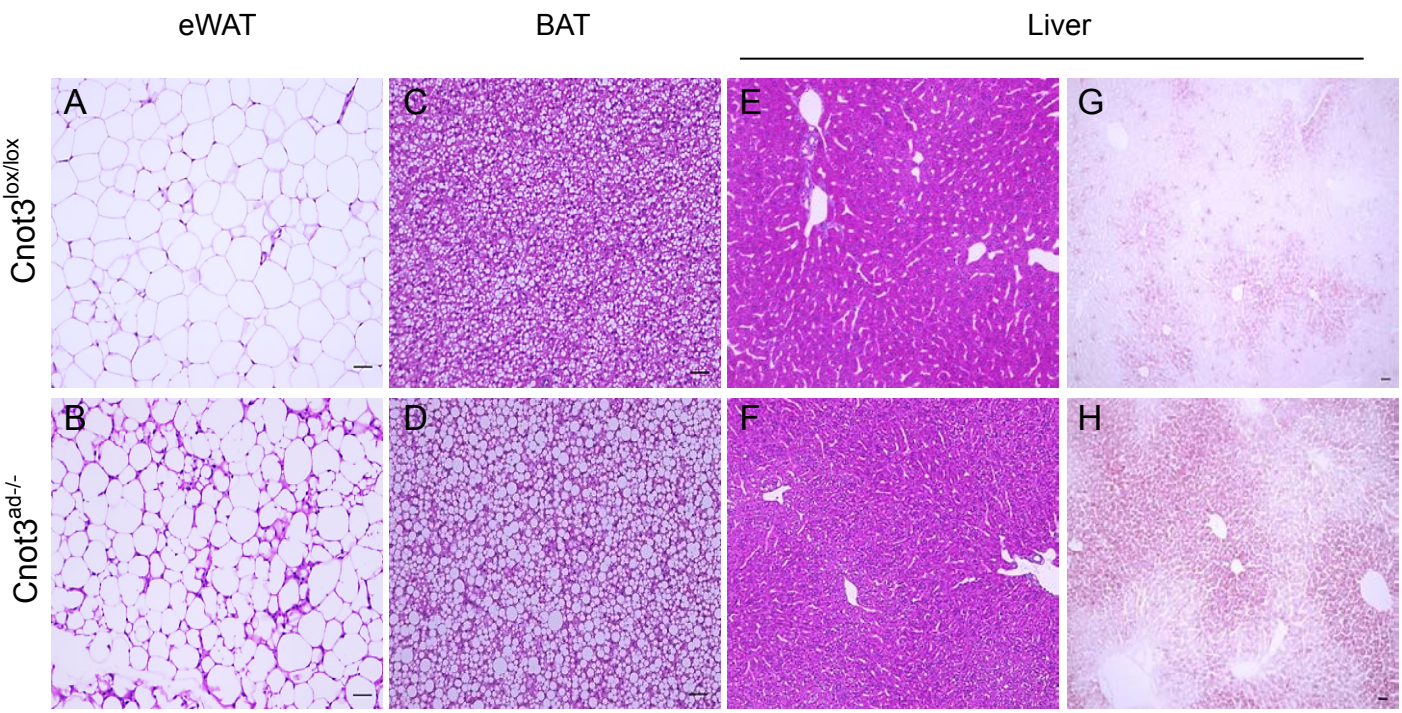

Figure 8. An abnormal lipid accumulation in the liver and BAT of *Cnot3*$^{ad-/-}$ mice. Histologic sections of WAT BAT and liver of 8-week-old wild type and *Cnot3*$^{ad-/-}$ mice. (A-F), HE staining of WAT BAT and liver, (G,H) oil-red-O staining of liver. Scale bar, 100μm.

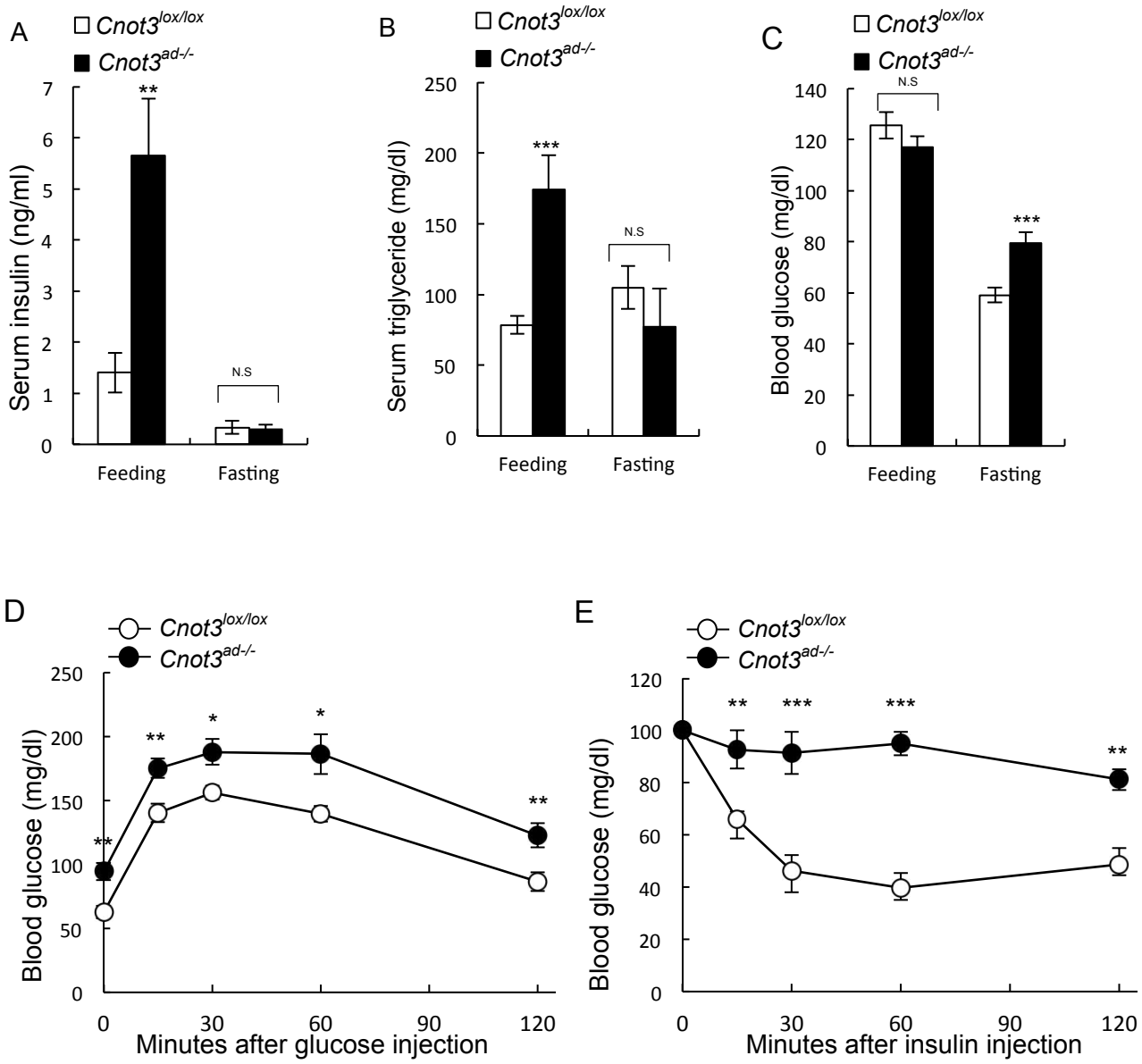

Figure 9. Typical metabolic sequelae of lipodystrophy in *Cnot3*$^{ad-/-}$ mice. (A) Serum insulin concentration (B) Serum triglyceride concentration (C) Blood glucose levels in fed or fasted *Cnot3*$^{lox/lox}$ and *Cnot3*$^{ad-/-}$ mice. (D and E) Glucose tolerance tests (GTTs) (D) and Insulin tolerance tests (ITTs) (E) in wild-type and *Cnot3*$^{ad-/-}$ mice fed on ND. Blood glucose levels were measured at each indicated time point following intraperitoneal injection of 0.5 g glucose per kg body weight or 1.0 U insulin per kg body weight. *n*=6–10 for each genotype. Results expressed as mean ± SEM, *p < 0.05, * * p < 0.01, * * * p < 0.001.

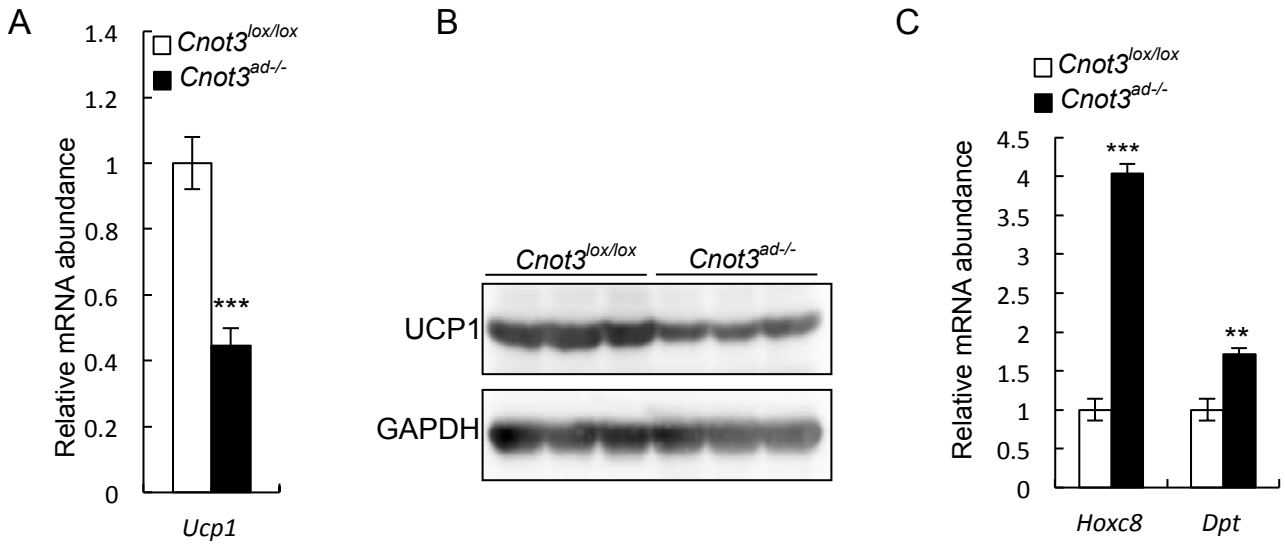

Figure 10. (A) qRT-PCR analysis of *Ucp1*mRNA expression level in BAT of *Cnot3*$^{ad-/-}$ mice and their wild-type littermates. (B) UCP1 protein expression level in BAT of *Cnot3*$^{ad-/-}$ mice and their wild-type littermates. (C) qRT-PCR analysis of *HoxC8* and *Dpt* in BAT of *Cnot3*$^{ad-/-}$ mice and their wild-type littermates.*P<0.05; **P<0.01 and ***P<0.001.

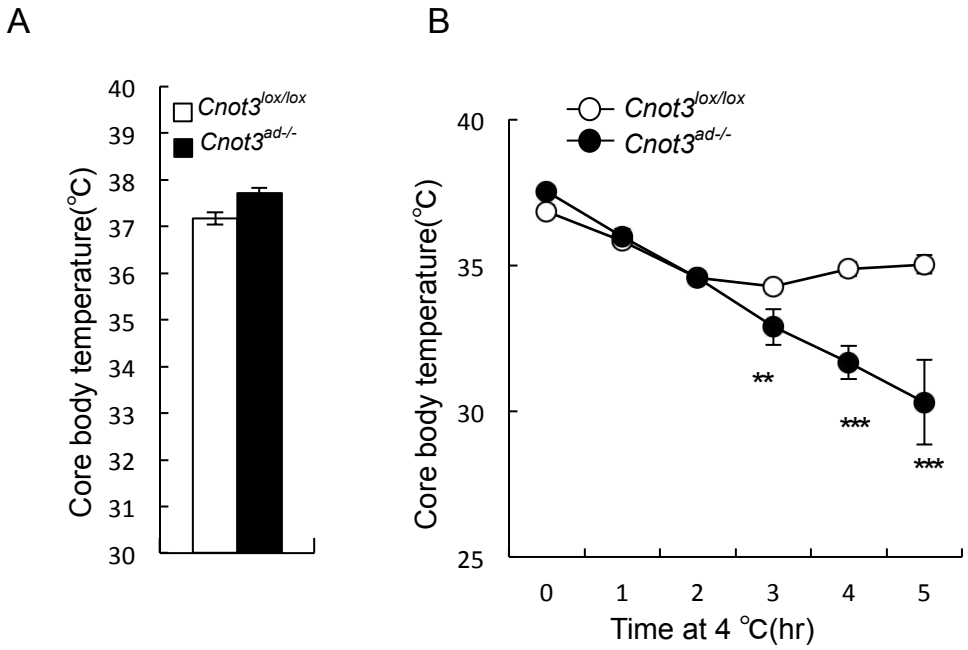

Figure 11. *Cnot3* deficiency impaired acute cold-induced thermogenesis.(A) Core body temperature of *Cnot3*$^{ad-/-}$ mice and their wild-type littermates. (B) Time course of core body temperature of *Cnot3*$^{ad-/-}$ mice and their wild-type littermates housed at 4°C. *n*=5 for each genotype. *P<0.05; **P<0.01 and ***P<0.001.

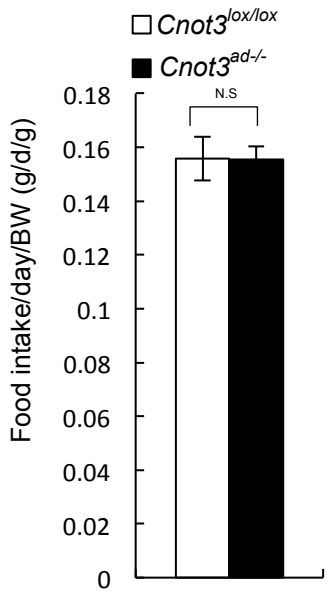

Figure 12. Average daily food was no different between *Cnot3*$^{ad-/-}$ mice and their wild-type littermates. Average daily food intake normalized to body weight. Daily food intake per mouse was measured over 7 days. *n*=10 for each genotype. *n*=10 for each genotype.

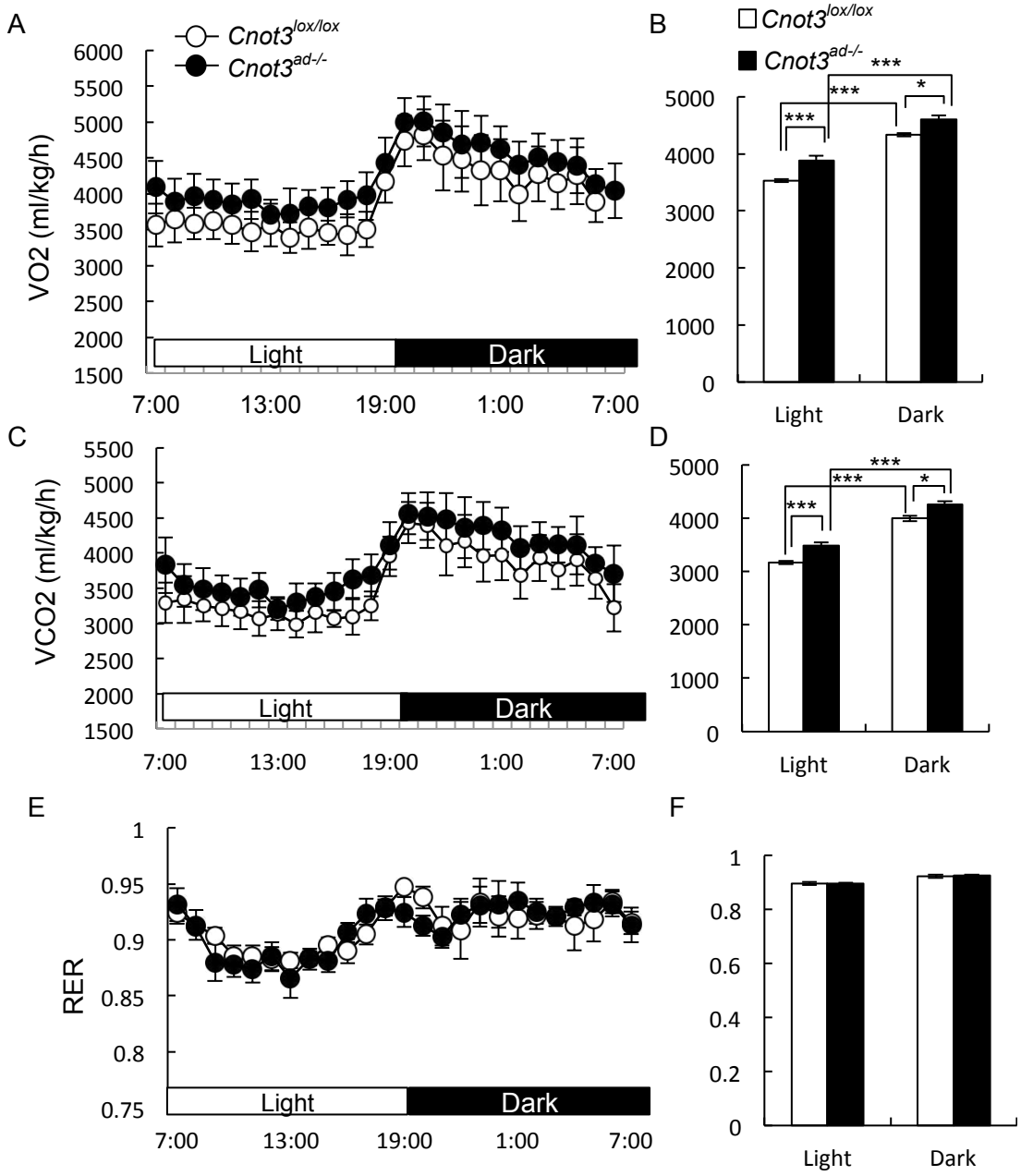

Figure 13. Increased energy expenditure in *Cnot3*$^{ad-/-}$ mice. (A and B) Oxygen consumption (VO_2) over 24 hr (A) and average VO_2 (B) in wild-type and *Cnot3*$^{ad-/-}$ mice fed on ND. (C and D) CO2 production (VCO_2) over 24 hr (C) and average VCO_2 (D) in wild-type and *Cnot3*$^{ad-/-}$ mice fed on ND. (E and F) Respiration exchange ratio (RER) over 24 hr (E) and average RER (F) in wild-type and *Cnot3*$^{ad-/-}$ mice fed on ND. The data were normalized to body weight. n = 4 per group. (C and D) respiratory exchange ratio (RER) . n = 4 per group. *p < 0.05, **p < 0.01 *** p < 0.001

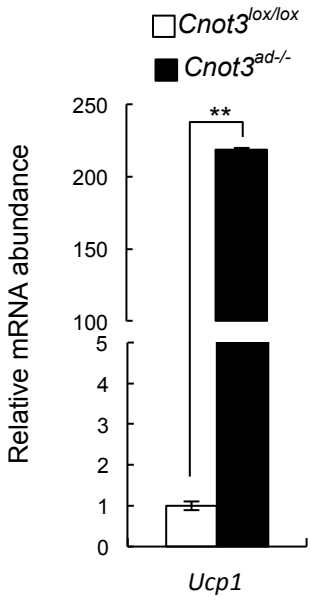

Figure 14. *Cnot3*$^{ad-/-}$ mice exhibited symptoms of cold stress even at 22°C. qRT-PCR analysis of *Ucp1*mRNA expression level in epididymal WAT of *Cnot3*$^{ad-/-}$ mice and their wild-type littermates. *n*=5 for each genotype. *P<0.05; **P<0.01 and ***P<0.001.

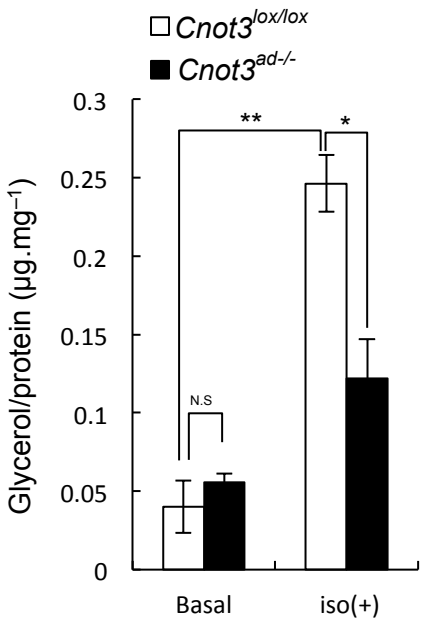

Figure 15. *Cnot3*$^{ad-/-}$ mice exhibited decreased lipolysis in vitro. (A) Rate of lipolysis in isolated adipocytes. Adipocytes were isolated from epididymal fat of male *Cnot3*$^{ad-/-}$ mice and their wild-type littermates. Glycerol was measured in the absence and presence of 10 mM of isoproterenol. *n*=4 for each genotype. Results are expressed as mean ± SEM, *p < 0.05, * * p < 0.01, * * * p < 0.001 (n = 4).

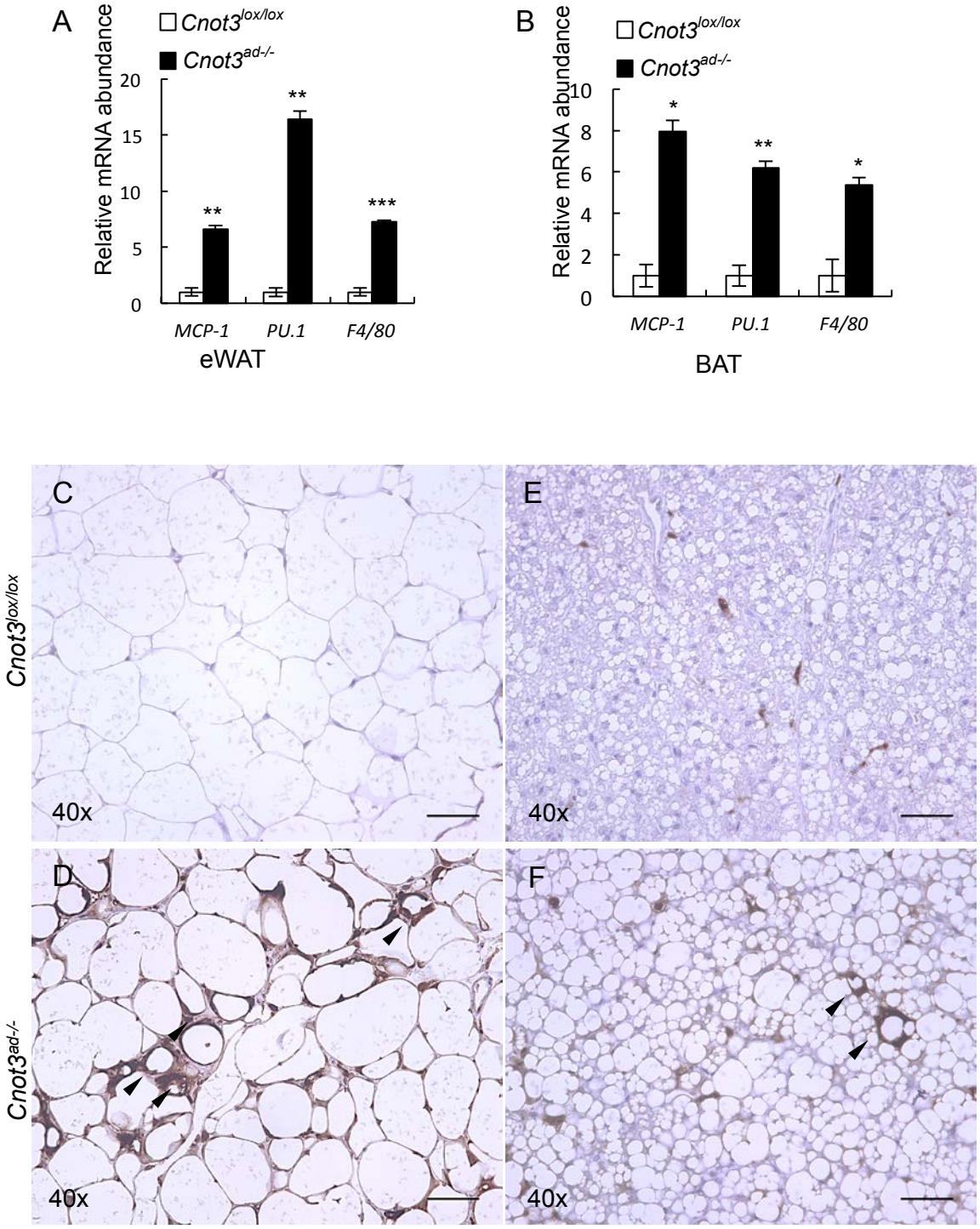

Figure 16. Inflammation and macrophages in adipose tissues of *Cnot3*$^{ad-/-}$ mice. Quantitative RT-PCR analysis of MCP-1 PU.1 and F4/80 in WAT (A) BAT(B) of *Cnot3*$^{ad-/-}$ mice and their wild-type littermates. Histological sections of epididymal WAT and BAT from 8 weeks old male *Cnot3*$^{ad-/-}$ and WT littermate. Immunohistochemical localization of macrophages in epididymal WAT(C,D) and BAT (E,F), arrowhead indicates crown-like structures (CLS). *P<0.05; **P<0.01 and ***P<0.001. Scale bar, 100μm.

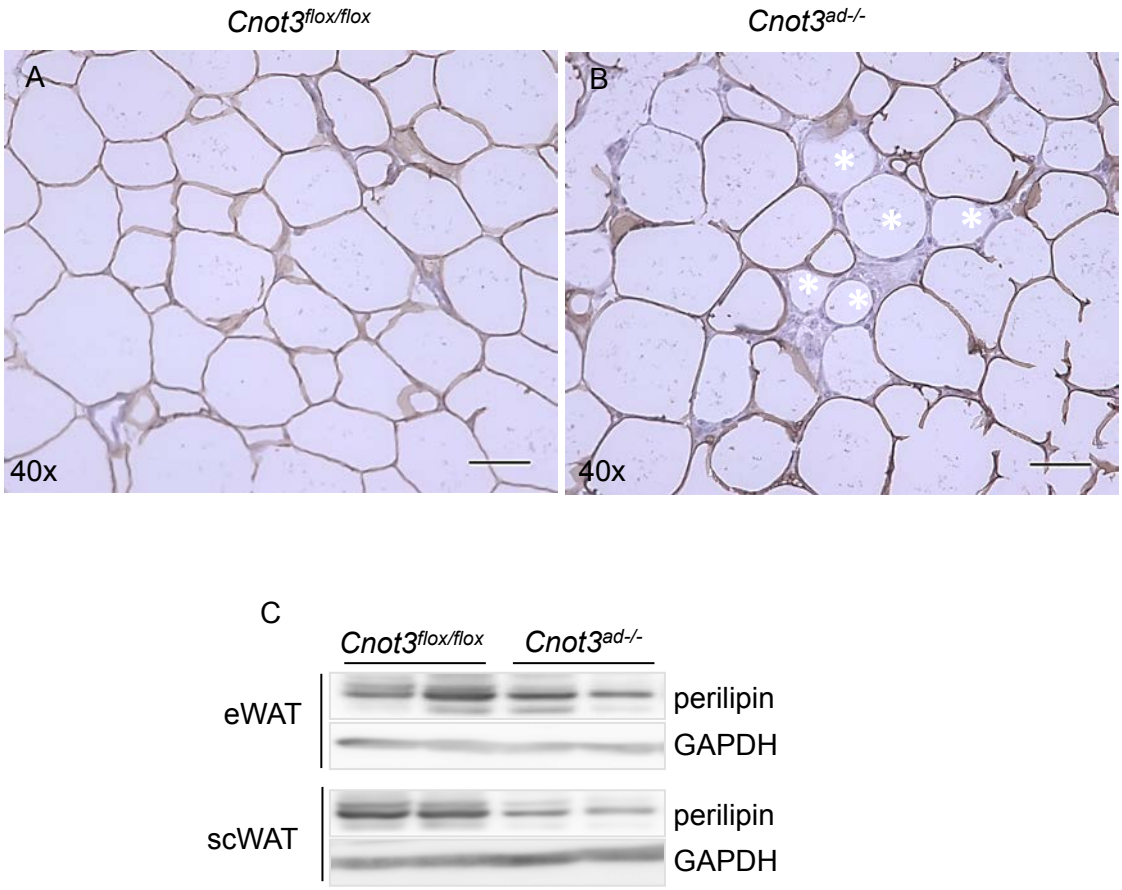

Figure 17. Adipocytes cell death in WAT of *Cnot3*$^{ad-/-}$ mice. (A,B)Histological sections of epididymal WAT from 8 weeks old male *Cnot3*$^{ad-/-}$ and WT littermate. Sections were stained with anti-perilipin antibody followed by colorimetric detection (brown) and counterstaining with hematoxylin (blue). White asterisk indicates dying adipocytes with perilipin-negative lipid droplets. Scale bar, 100µm. (C) Protein expression levels in WAT.

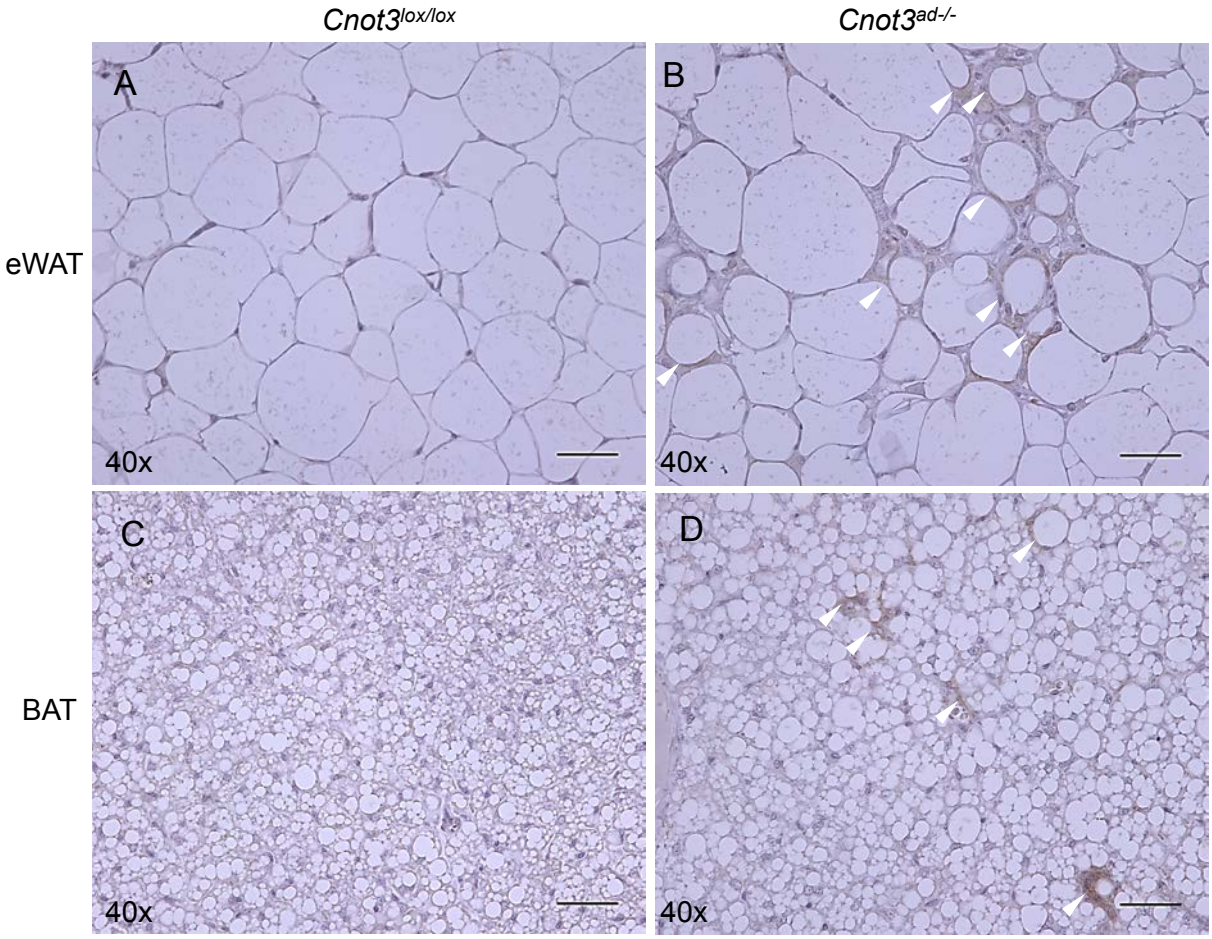

Figure 18. Adipocytes apoptosis. Histological sections stained for apoptosis with anti-cleaved caspase 3 antibody (brown) and counterstaining with hematoxylin (blue) in epididymal WAT(A,B) and BAT (C,D). Arrowhead indicates adipocytes with activated capase 3. Scale bar, 100μm.

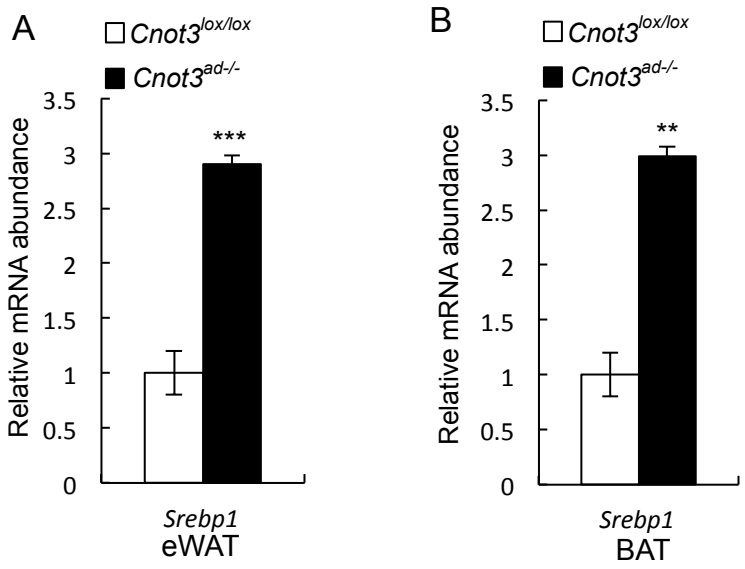

Figure 19. The expression level of *Srebp1* were significantly up-regulated in both WAT and BAT of *Cnot3*$^{ad-/-}$ mice. qRT-PCR analysis of *Srebp1*mRNA expression level in WAT(A)and BAT (B) of *Cnot3*$^{ad-/-}$ mice and their wild-type littermates. *P<0.05; **P<0.01 and ***P<0.001.

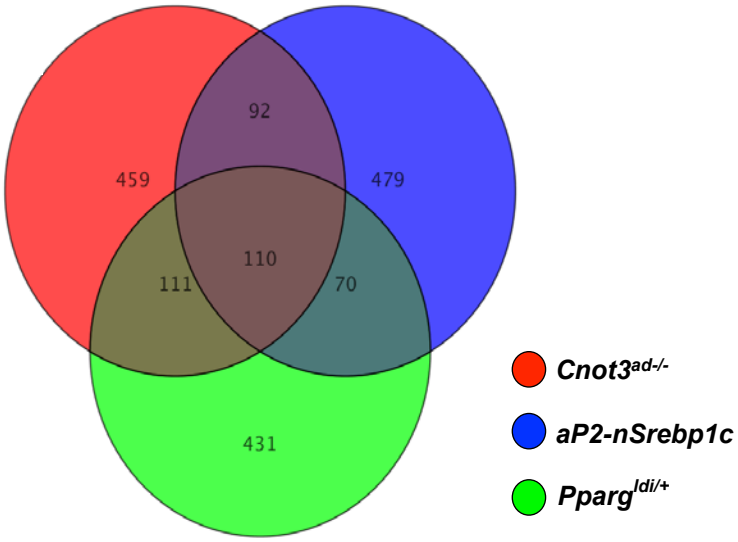

Figure 20. Overlapping gene expression in *Cnot3*$^{ad-/-}$, *aP2-nSrebp1c* and *Pparg*$^{ldi/+}$ fat. Venn diagram depicting the numbers of overlapping and strain specific genes that are upregulated more than 2.5-fold in these strains.

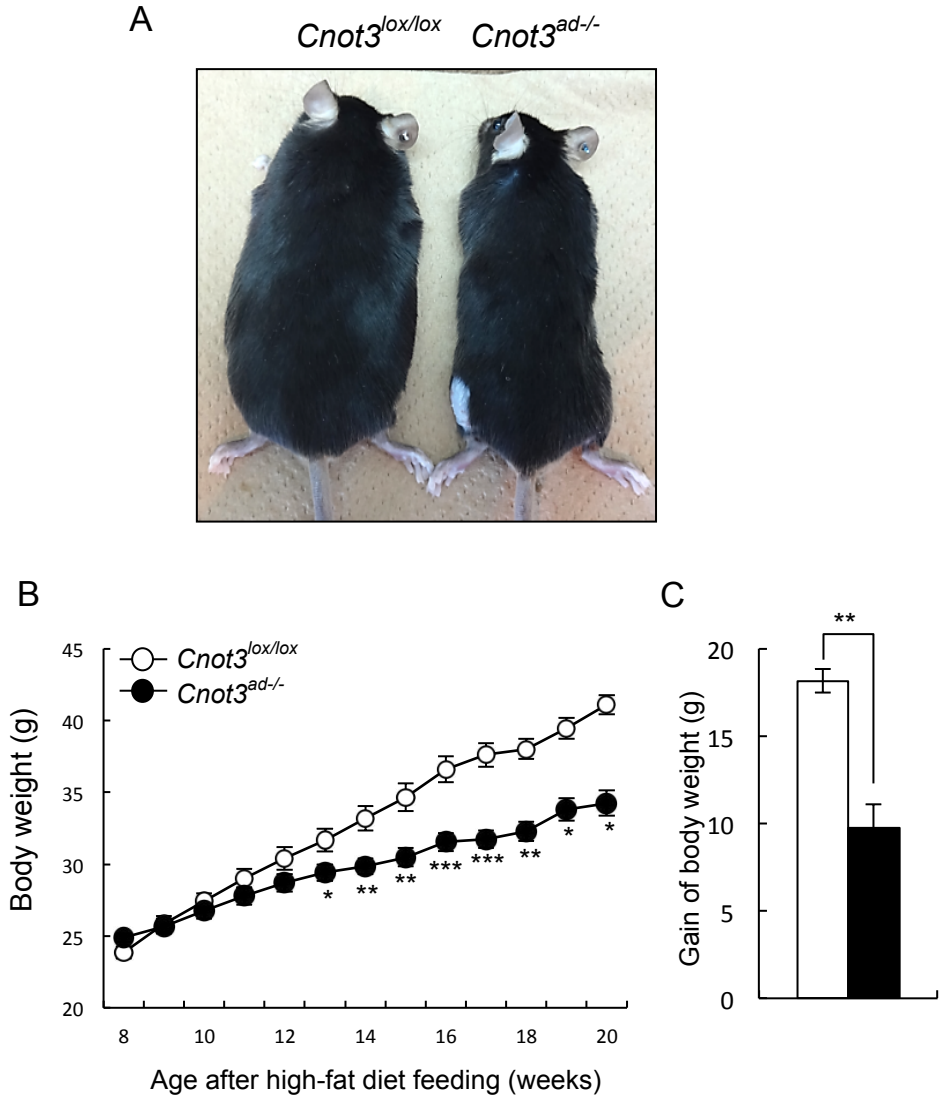

Figure 21. Resistance to high-fat diet-induced obesity. (A) Gross appearance and (B) growth curve of 20-week-old *Cnot3*$^{ad-/-}$ mice and their wild-type littermates after HFD feeding. (C) Gains of body weight of wild-type and *Cnot3*$^{ad-/-}$ mice were calculated from (B). *n*=10 for each genotype. *P<0.05; **P<0.01 and ***P<0.001.

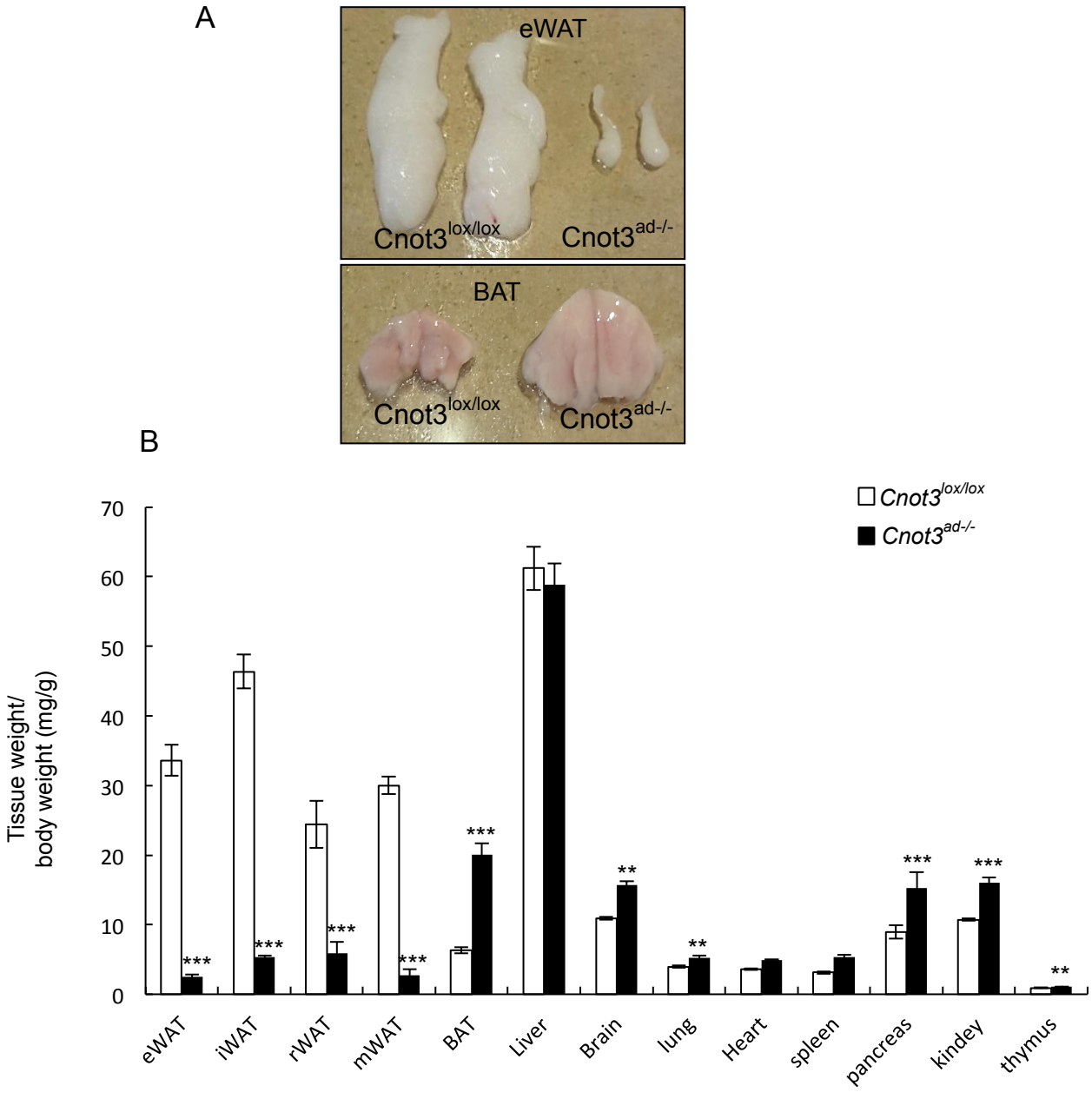

Figure 22. Exacerbated lipodystrophy in HFD-fed *Cnot3*$^{ad-/-}$ mice. (A) Fat pads morphology of wild-type and *Cnot3*$^{ad-/-}$ mice. (B) The relative weight of the indicated organs. The weight of the organ was normalized to body weight. *n*=10 for each genotype. *P<0.05; **P<0.01 and ***P<0.001.

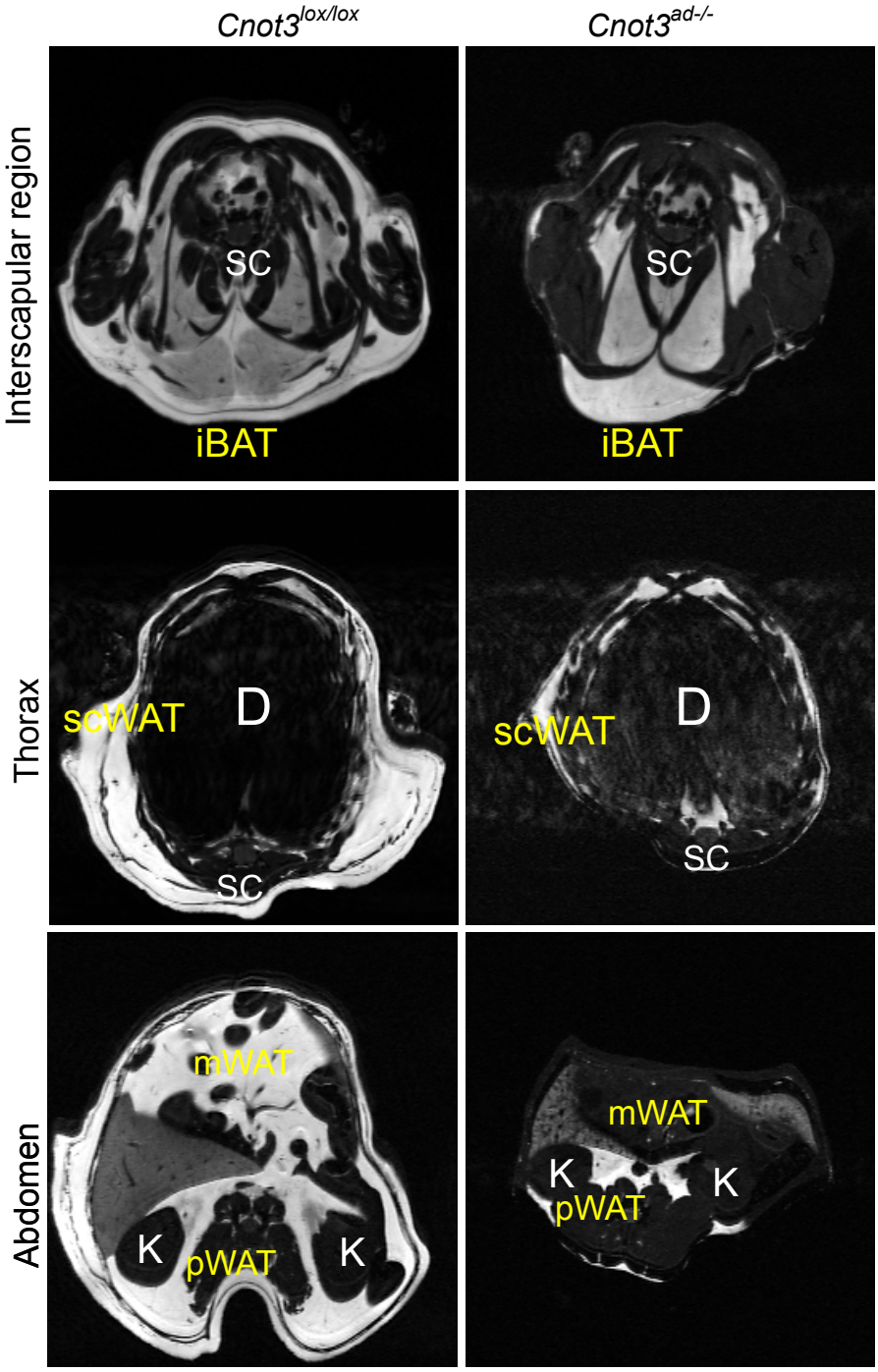

Figure 23. MRI imaging of wild-type (left) and *Cnot3*$^{ad-/-}$ (right) mice after 12 weeks on HFD feeding. Cross-section at the level of the interscapular region (A), thorax (B) and abdomen (C). D, diaphragm; scWAT, subcutaneous WAT; mWAT, mesenteric WAT; pWAT, retroperitoneal fat; BAT , Interscapular BAT; SC, spinal cord;. K, kidney.

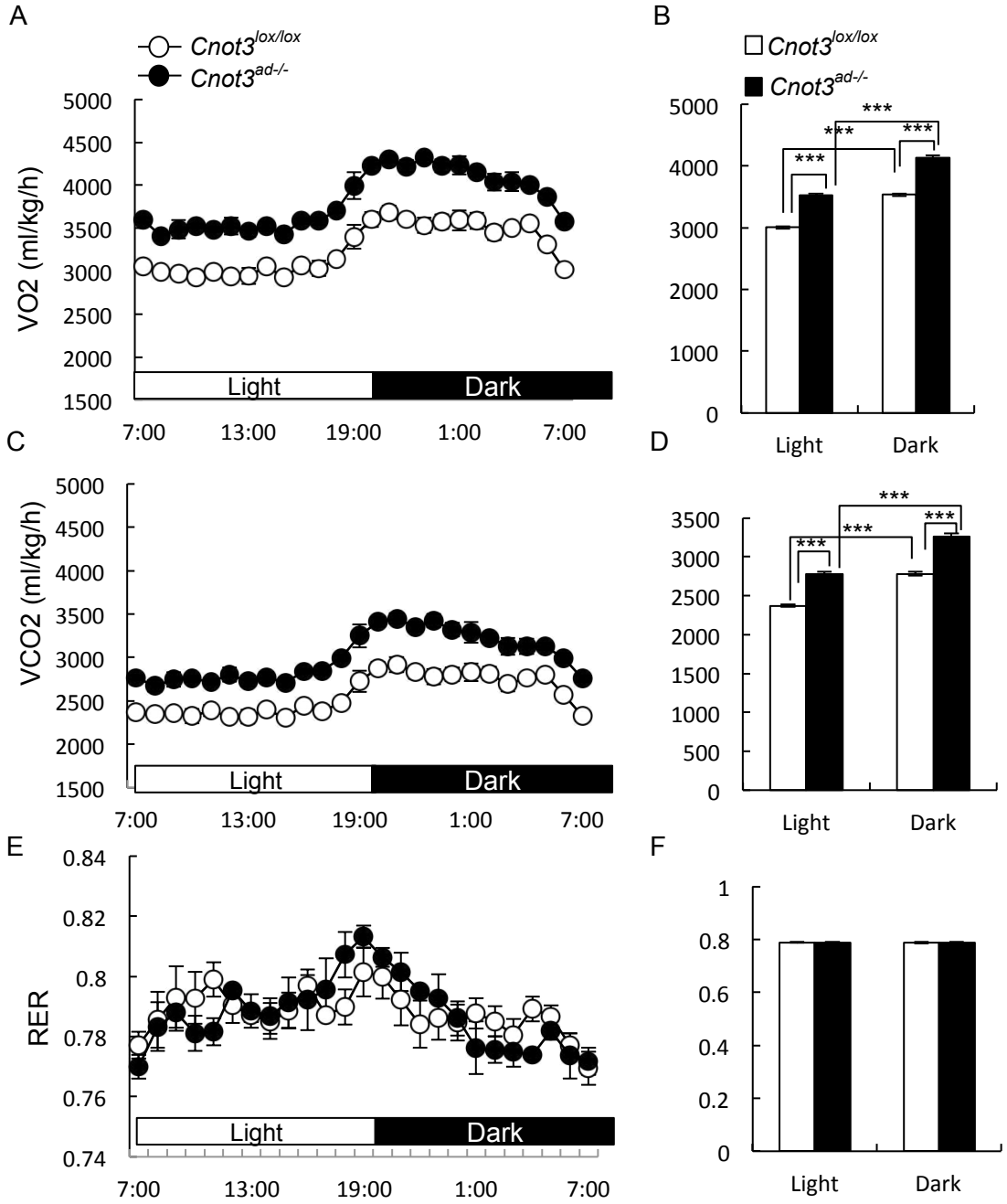

Figure 24. Increased energy expenditure in HFD-fed *Cnot3*$^{ad-/-}$ mice. (A and B) Oxygen consumption (VO_2) over 24 hr (A) and average VO_2 (B) in wild-type and *Cnot3*$^{ad-/-}$ mice fed on HFD. (C and D) CO2 production (VCO_2) over 24 hr (C) and average VCO_2 (D) in wild-type and *Cnot3*$^{ad-/-}$ mice fed on HFD. (E and F) Respiration exchange ratio (RER) over 24 hr (E) and average RER (F) in wild-type and *Cnot3*$^{ad-/-}$ mice fed on HFD. The data were normalized to body weight. n = 4 per group. (C and D) respiratory exchange ratio (RER) . n = 4 per group. *p < 0.05, **p < 0.01 *** p < 0.001

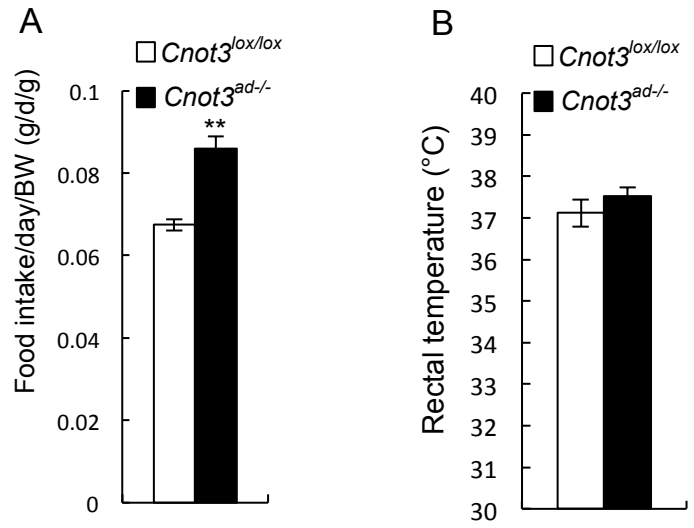

Figure 25.(A) Average daily food intake normalized to body weight. Daily food intake per mouse was measured over 7 days. *n*=10 for each genotype. (B) Rectal temperature of *Cnot3*$^{ad-/-}$ mice and their wild-type littermates under HFD feeding. *n*=10 for each genotype

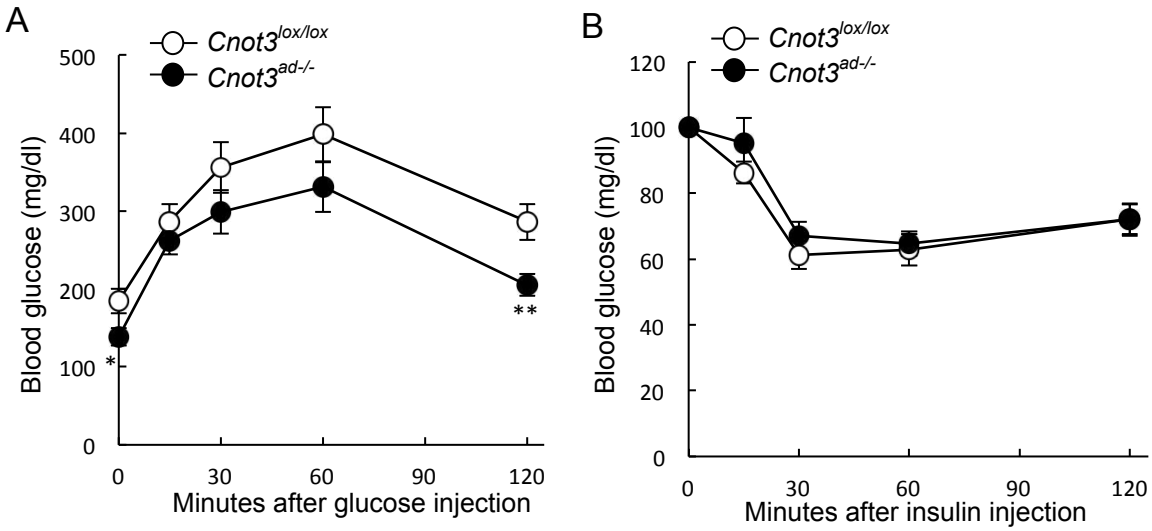

Figure 26. The resistance to diet-induced obesity exhibited by HFD-fed *Cnot3*$^{ad-/-}$ mice did not prevent the severe insulin resistance. Glucose tolerance tests (GTTs) (A) and Insulin tolerance tests (ITTs) (B) in wild-type and *Cnot3*$^{ad-/-}$ mice fed on HFD. Blood glucose levels were measured at each indicated time point following intraperitoneal injection of 0.5 g glucose per kg body weight or 1.0 U insulin per kg body weight. n=8–10 for each genotype. Results expressed as mean ± SEM, *p < 0.05, * * p < 0.01, * * * p < 0.001.

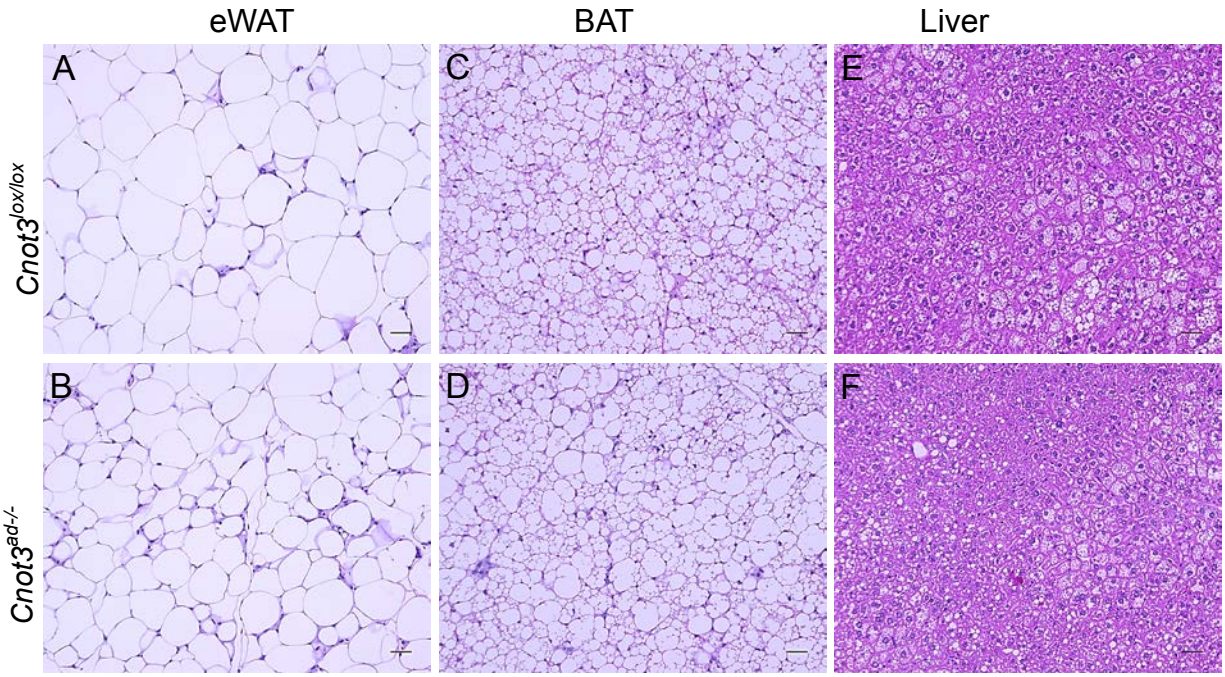

Figure 27. HFD-fed *Cnot3*$^{ad-/-}$ mice were resistant to obesity but lipid accumulation levels in adipose tissues and liver were not improved. Histologic sections of WAT (A,B), BAT (C,D), and liver (E,F), of wild type and *Cnot3*$^{ad-/-}$ mice after 12 weeks HFD feeding. Scale bar, 100μm.

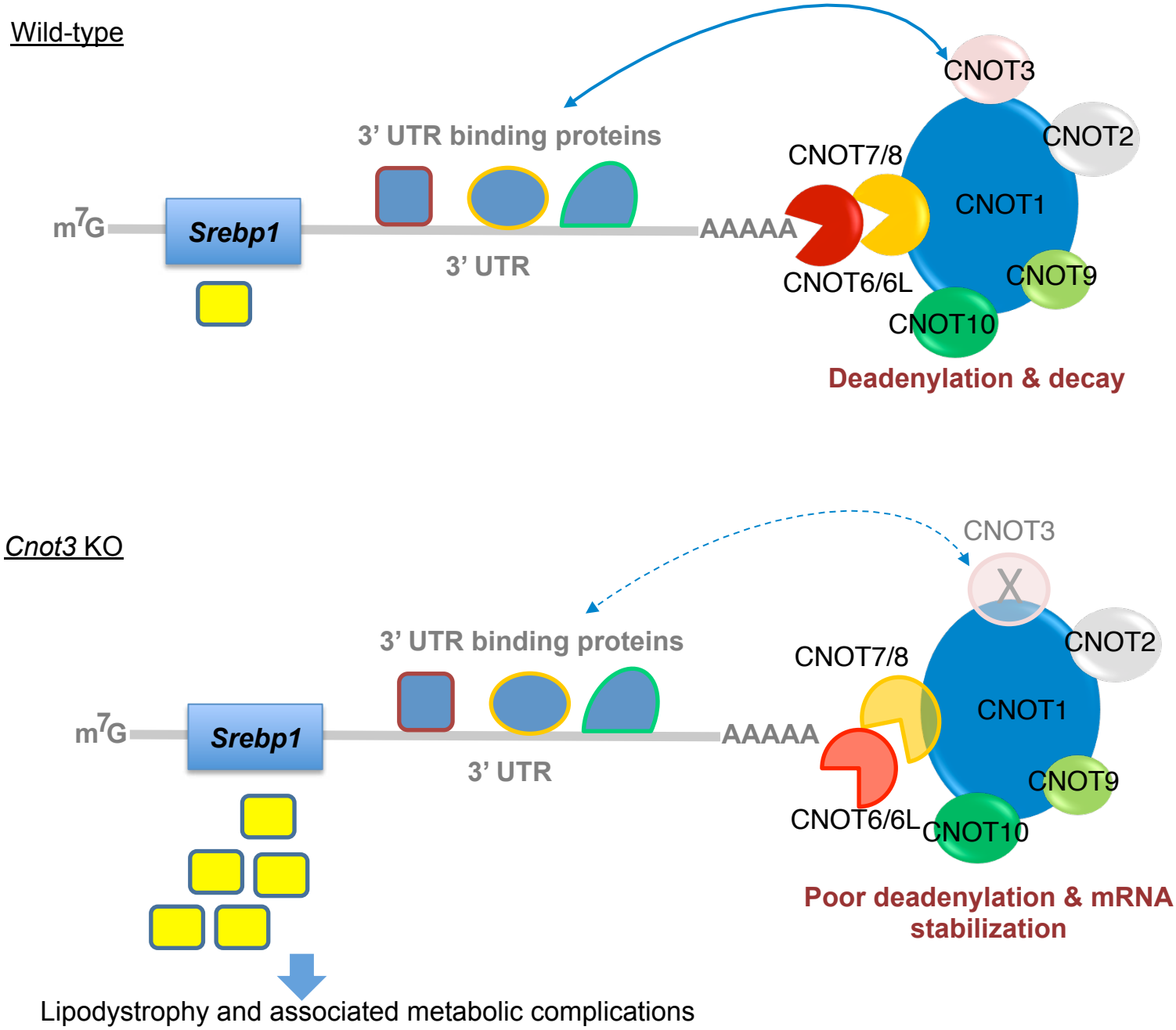

Figure 28. Model of possible involvement of CNOT3 in specific mRNA decay. In *Cnot3*-deficient adipose tissue, degradation of mRNA related to lipodystrophy such as *Srebp1* is not completely triggered, resulting in lipodystrophy and associated metabolic complications.

Table 1

Pathway	p-value
Activation of Gene Expression by SREBP (SREBF)	3.33E-09
Mm_Chemokine_signaling_pathway_WP2292_51127	6.59E-07
Mm_B_Cell_Receptor_Signaling_Pathway_WP274_41374	3.33E-06
Mm_T_Cell_Receptor_Signaling_Pathway_WP480_41339	1.87E-05
Mm_IL-5_Signaling_Pathway_WP151_41364	3.14E-05
Mm_Type_II_interferon_signaling_(IFNG)_WP1253_48389	1.37E-04
Mm_IL-3_Signaling_Pathway_WP373_41387	2.37E-04
Role of DCC in regulating apoptosis	0.003242
The AIM2 inflammasome	0.003728
Mm_IL-2_Signaling_Pathway_WP450_41330	0.005688
Mm_Apoptosis_WP1254_47965	0.009578
Mm_IL-6_signaling_Pathway_WP387_41281	0.025416
Mm_IL-1_Signaling_Pathway_WP37_41331	0.041963
Mm_IL-4_signaling_Pathway_WP93_41293	0.066369

Table 2 List of primer sequences for qRT-PCR analysis

Gene	Forward primer	Reverse primer
Leptin	TCAAGCAGTGCCTATCCAGA	AAGCCCAGGAATGAAGTCCA
Pparg1	TGAAAGAAGCGGTGAACCACTG	TGGCATCTCTGTGTCAACCATG
Pparg2	GTTTTATGCTGTTATGGGTG	GTAATTTCTTGTGAAGTGCTCATAG
Cebpa	AAACAACGCAACGTGGAGA	GCGGTCATTGTCACTGGTC
Cebpb	TGATGCAATCCGGATCAA	CACGTGTGTTGCGTCAGTC
Fabp4	GAAAACGAGATGGTGACAAGC	GCCCTTTCATAAACTCTTGTGG
Lpl	GAAAGCCGGAGAGACTCAGA	TGGCATTTCACAAACACTGC
Fasn	GGCTGAGGCCTTATGCTTCT	CGATCTTCCAGGCTCTTCAG
Adipoq	GATGGCACTCCTGGAGAGAA	CAGCTCCTGTCATTCCAACA
Mcp1	TCCCAATGAGTAGGCTGGAG	AAGTGCTTGAGGTGGTTGTG
PU.1	CGGATGTGCTTCCCTTATCAAAC	TGACTTTCTTCACCTCGCCTGTC
F4/80	CTGTAACCGGATGGCAAACT	CTGTACCCACATGGCTGATG
Cidea	AAACCATGACCGAAGTAGCC	AGGCCAGTTGTGATGACTAAGAC
Pgc1a	GAAAGGGCCAAACAGAGAGA	GTAAATCACACGGCGCTCTT
UCP1	CTGCCAGGACAGTACCCAAG	TCAGCTGTTCAAAGCACACA
Prdm16	GACATTCCAATCCCACCAGA	CACCTCTGTATCCGTCAGCA
HoxC8	GTCTCCCAGCCTCATGTTTC	TCTGATACCGGCTGTAAGTTTGT
HoxC9	GCAGCAAGCACAAAGAGGAGAAG	GCGTCTGGTACTTGGTGTAGGG
DPT	CTGCCGCTATAGCAAGAGGT	TGGCTTGGGTACTCTGTTGTC
Pref1	AGTACGAATGCTCCTGCACAC	CTGGCCCTCATCATCCAC
Srebp1	TGGAGACATCGCAAACAAG	GGTAGACAACAGCCGCATC
36B4	ACTGGTCTAGGACCCGAGAAG	TCCCACCTTGTCTCCAGTCT

Table 3. Common alterations in gene expression between *Cnot3*$^{ad-/-}$ mice, *aP2-nSrebp1c* mice (*Sr*) and *Pparg*$^{ldi/+}$ mice

Gene Symbol	***Cnot3***$^{ad-/-}$	***Sr***	***Pparg***$^{ldi/+}$
Atp6v0d2	33.08762	9.810689	9.586352
Atp6v0d2	24.53461	15.216072	6.5242734
Ubd	22.24502	18.176474	4.8160057
Gpnmb	21.43772	10.154126	6.1500793
Mmp12	20.477654	7.7889333	8.49861
Rgs1	18.15279	9.656038	6.8217173
Adam8	14.653106	3.293955	4.1736326
BC090627///Chkb///Cpt1b	13.505972	2.8459737	4.778608
Rnf128	12.480404	11.810144	4.8790584
Ptx3	12.312386	2.6123056	4.572586
Clec4d	11.105232	10.539208	5.4622436
Myo1f	10.51756	5.8811235	9.545781
Gas2l3	9.792868	3.3634965	5.0809913
Slc15a3	9.634179	4.966626	6.6345215
Nceh1	8.897664	5.2589817	4.1819267
Glipr1	8.622081	4.387046	4.4066997
Slc37a2	8.281363	8.818674	3.2722108
Rnf128	8.186457	13.052683	5.5072045
Hpgds	8.068502	5.2188573	5.353414
Hephl1	8.053279	11.273928	3.112512
LOC100038947///Sirpb1a///Sirpb1b	7.708848	6.73981	9.267849
Il7r	7.395923	4.7066603	5.1543264
Stap1	7.374021	3.4476826	4.9083214
Saa3	7.1283875	3.304791	5.85182
Egr2	6.880793	3.165907	4.2676663
Gas2l3	6.878086	8.23601	5.721606
Cd84	6.8606653	3.9313505	4.3929043
Cd300lb	6.237835	2.9473276	3.7715843
	6.2352467	2.6469953	4.82692

Gp49a///Lilrb4	5.9790707	5.354253	4.2251782
Syngr1	5.943864	3.2444184	2.8738883
Tnfaip2	5.7677865	4.211666	2.648325
Sel1l3	5.6567383	4.062649	2.6104815
Sirpb1a	5.6034284	4.10811	4.569261
Ms4a7	5.573173	6.3547072	8.929953
Dhcr7	5.483312	9.554989	2.6028285
Itgb2	5.3336196	3.707813	3.4741802
AF251705	5.313738	4.7287655	4.860008
	5.281763	4.800038	5.609574
Atf3	5.249977	3.2650237	4.30438
Tlr13	5.2391863	3.4600484	4.1681376
Fcgr1	5.1961966	3.5480723	5.575852
Myo1f	5.1530848	3.4528615	3.3839786
Soat1	5.0243497	2.9990659	2.655846
C3ar1	5.0050144	5.396723	4.38334
Vsig4	4.9685345	4.946934	3.8997986
Nceh1	4.952117	2.8143167	3.0553768
Lipa	4.8687444	4.422588	3.1223793
Lpxn	4.844463	3.3294284	4.3958635
Sh3bgrl2	4.821051	8.904034	3.0627503
Blnk	4.73978	2.598941	3.4694054
Lcp1	4.719951	3.033085	3.9179642
Hk3	4.474945	7.4301524	3.9512708
Il1rn	4.385892	2.7079923	3.2642322
Adssl1	4.3647285	3.6326184	4.2141976
Gla	4.3517866	5.6278105	2.7533383
Ms4a6d	4.296815	4.353101	7.5985646
Plek	4.2887893	4.299423	4.367061
Cxcl2	4.2763424	5.481742	4.005331
Ccl8///LOC100503254	4.2554717	6.720313	8.293636
Tyrobp	4.225148	2.8367	3.7948747

Mpeg1	4.2040443	5.36486	6.068006
Runx2	4.183405	3.0392432	2.665151
Cd44	3.9880695	2.5492945	4.0930285
Arhgap25	3.9607818	2.7931817	3.4228747
Soat1	3.9504743	4.71612	2.5526962
Cadm1	3.8520896	2.522139	4.3380046
Emr1	3.8295417	3.307787	3.1338458
Bcl2a1a///Bcl2a1b///Bcl2a1d	3.819242	3.5564747	5.528718
Clec4a2	3.8116543	2.930638	4.5165434
Evi2a	3.7805014	2.701513	3.4836273
Ctss	3.7668247	3.1078336	3.6910787
Lipa	3.6363273	3.9490979	3.0024137
Lgals3	3.610286	2.6200294	2.804145
Plac8	3.5879545	4.244216	7.493948
Ifi30	3.5301251	3.065401	4.1522775
Fmn1	3.519733	4.305155	3.1109025
Trav9d-3	3.5102053	2.7723846	4.3916216
Mreg	3.4713526	4.8967347	3.4062834
Tpd52	3.4615855	3.290438	3.2672234
Tpd52	3.444644	2.6440835	2.9244926
Apobec1	3.436342	4.5847936	3.875408
Ms4a6d	3.4309351	4.732254	6.3539133
Rasgef1b	3.4305656	2.798825	2.7915344
Clec7a	3.4205937	3.569485	3.5505793
Cd72	3.4196198	2.9965196	7.9505415
Cdt1	3.404903	2.964215	2.8823097
Plek	3.3843572	4.2045627	3.1005783
Lair1	3.380313	3.0466354	6.4997187
Soat1	3.3737845	3.2053733	2.8246162
Hk3	3.307934	3.0944223	3.2940066
Basp1	3.2674203	2.6278448	2.53381
Ms4a4c	3.1970384	3.6948576	8.713206

Galnt6	3.191125	3.130455	2.7094235
Tlr1	3.1484253	4.228831	4.6859097
Capn9	3.1380696	2.9420402	3.3880258
	3.1214275	3.3966806	4.4317026
Evl	3.1099327	3.277143	3.0488527
Naip2	3.0912554	5.093412	4.155447
Cd48	3.0730634	2.8741891	3.4370227
Cd53	3.0332565	2.689707	3.3658493
Casp1	3.0104728	4.8834686	4.9914384
Gm11428///LOC100504934	2.9978454	2.941623	3.161411
Nckap1l	2.7658994	2.503009	2.9571748
Fyb	2.6945875	3.6301687	4.3732305
Fcgr4	2.6935823	7.2860966	6.34155
Chchd10	2.6695423	3.569411	3.5217676
Oasl1	2.6294043	7.7111597	2.8229966
Msr1	2.616367	2.668048	5.051168
Gpr65	2.5295546	3.2761838	5.5563107